

UNIVERSITY OF MELBOURNE

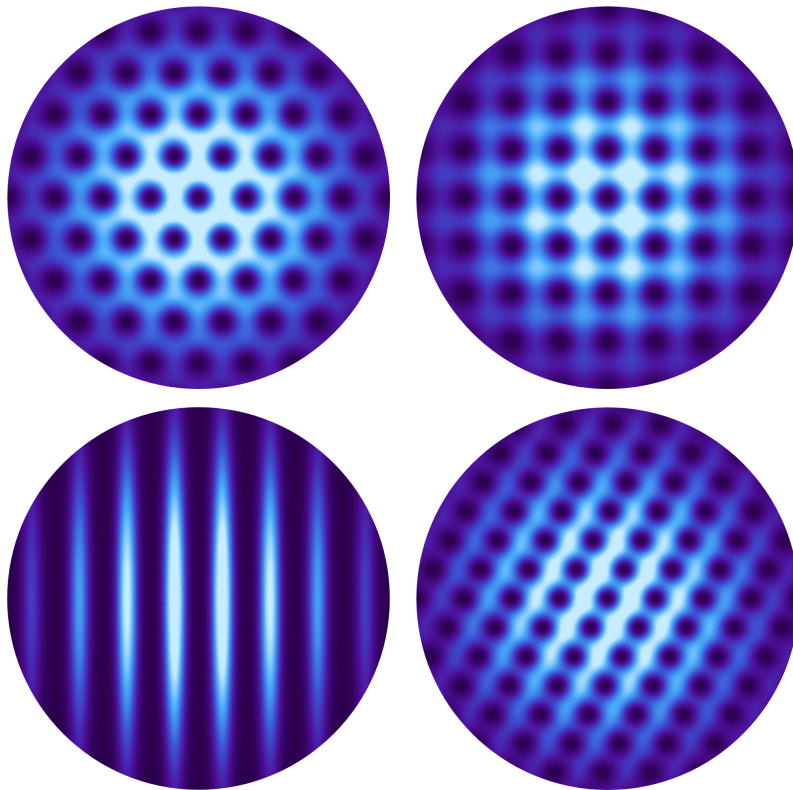
Vortex Lattices in Quasi-Two-Dimensional Dipolar Bose-Einstein Condensates

Author:

Neil Marchant

Supervisor:

Dr. Andy Martin



*A thesis submitted in partial fulfilment of the requirements
for the degree of Master of Science.*

October 2014

Abstract

We develop a variational method for analysing vortex lattice geometry in quasi-two-dimensional dipolar BECs in the fast-rotating limit. The vortex lattice geometry is found to depend on the relative strength of the contact versus dipolar interactions, ϵ_{dd} , as well as the angle of the dipole polarisation α . In the region of the $(\epsilon_{\text{dd}}, \alpha)$ parameter space where the effective local interactions dominate ($1/\epsilon_{\text{dd}} \gtrsim 1$), we find that the vortex lattice geometry is triangular, as is the case in non-dipolar BECs. However, in regions where the effective non-local interactions become significant ($-1 \lesssim 1/\epsilon_{\text{dd}} \lesssim 1$), we find that the vortex lattice geometry is square or rectangular. For the case of on-axis polarisation ($\alpha = 0$), we find that triangular, square and rectangular vortex lattice geometries are possible. However, as the polarisation is tilted off-axis (α is increased above zero), the rectangular lattice geometry eventually ceases to exist. These results qualitatively agree with two previous studies for the case of on-axis polarisation ($\alpha = 0$) [1, 2]. Our results for the case of off-axis polarisation ($0 < \alpha \leq \frac{\pi}{2}$) are a new contribution to research in this area.

Statement of Contributions

Chapters 1 and 2 are an original review of relevant theory and past work in the field. Chapters 3, 4 and 5 contain my own theoretical work unless otherwise stated.

Acknowledgements

First and foremost, I would like to express my sincere appreciation and gratitude to my supervisor, Dr. Andy Martin, for his continuous encouragement, support and guidance throughout my M.Sc. studies.

I would also like to thank Dr. Brendan Mulkerin and Dr. Nick Parker for their valuable input and insightful discussions.

Contents

1	Introduction	1
1.1	A brief history of BEC	1
1.2	A theory of BEC: Gross-Pitaevskii theory	2
1.3	Inter-atomic interactions	3
1.4	Superfluidity and vortices in BECs	4
1.5	Vortex lattices	5
1.6	A new research problem	6
2	Vortex lattices in non-dipolar BECs	8
2.1	The energy functional for a rotating BEC in quasi-2D	8
2.2	Ansatz for the vortex lattice ground state	10
2.2.1	The lowest Landau level (LLL) state and a link to vortices	11
2.2.2	Mathematical description of the vortex lattice	12
2.2.3	Derivation of the vortex lattice ground state	13
2.3	Evaluation of the energy in the vortex lattice ground state	14
2.4	Optimal vortex lattice geometry	15
2.5	Summary	18
3	Vortex lattices in dipolar BECs with on-axis polarisation	19
3.1	Modifying the two-particle pseudo-potential	19
3.2	The dipolar interaction energy contribution in quasi-2D	20
3.3	Evaluation of the dipolar interaction energy contribution in the vortex lattice ground state	21
3.4	Solution to numerical issues	23
3.5	Optimal vortex lattice geometry	25
3.5.1	Preliminary setup	25
3.5.2	Results and discussion	26
3.6	Summary	27
4	Vortex lattices in dipolar BECs with off-axis polarisation	30
4.1	Parametrisation of the dipole polarisation	30
4.2	Re-evaluating the dipolar interaction energy contribution in the vortex lattice ground state	31
4.3	Optimal vortex lattice geometry	32

4.3.1	Dipole polarisation in the plane of rotation	33
4.3.2	Varying the dipole polarisation	34
4.4	Summary	35
5	Conclusions, ongoing and future work	37
5.1	Conclusions	37
5.2	Ongoing work	38
5.2.1	A new ansatz for the vortex lattice ground state	39
5.2.2	Re-evaluating the condensate energy	40
5.2.3	Optimal vortex lattice geometry	41
5.3	Future work	42
	Bibliography	43

Chapter 1

Introduction

1.1 A brief history of BEC

In a gas of atoms, the profound differences between bosons and fermions ordinarily have no observable effect on a macroscopic scale. In fact, it is often sufficient to describe such gases, even on a microscopic scale, using a classical theory such as statistical mechanics. At ultra-cold temperatures, however, the differences between bosons and fermions become apparent in a remarkable way through the phenomenon of *Bose-Einstein condensation (BEC)*. This phenomenon is characterised by macroscopic population of the lowest energy quantum state and is a unique consequence of the quantum statistical nature of bosons — it does not occur for the case of fermions.

BEC was first predicted to occur by A. Einstein in 1925 [3]. However, it wasn't until 70 years later, in 1995, that Einstein's prediction was verified experimentally for the first time in a dilute atomic gas. This first successful experiment was carried out by a group led by Cornell and Wieman using a gas of ^{87}Rb atoms cooled to 170 nK [4]. Ketterle's group followed shortly after with an observation of BEC in ^{23}Na atoms [5]. The success of these experiments was largely due to technological advances in cooling methods and magneto-optical trapping. Cornell, Wieman and Ketterle later received the 2001 Nobel Prize in Physics for their contributions to the study of BECs [6].

A more recent experimental development is the achievement of BEC in dipolar Bose gases, that is, gases of bosonic atoms or molecules which have strong magnetic or electric dipole moments. The first successful experiment of this kind was conducted in 2005 using a gas of ^{52}Cr atoms which have a magnetic dipole moment of about $6\mu_B$ [7]. This was an impressive experimental feat and required novel cooling techniques to deal with relaxation processes which occur due to the dipolar nature of the atoms. Since 2005, other experimental groups have achieved BEC using atomic species with even stronger magnetic dipole moments. Of particular interest is the achievement of BEC using ^{164}Dy which has a magnetic dipole moment of $10\mu_B$ [8]. In the ^{164}Dy BEC, the interactions between the magnetic dipole moments are so strong that they dominate over the usual van-der-Waals-like interactions. As such, this could lead to promising investigations of in the strongly dipolar regime.

1.2 A theory of BEC: Gross-Pitaevskii theory

In order to give an exact theoretical treatment of BEC, one must solve the quantum many-body problem for a Bose gas. This remains a formidable challenge with current technology (i.e. classical computers), because the size of the Hilbert space grows exponentially with the number of particles in the gas. Fortunately, however, many of the important properties of BECs may be investigated using low-order approximations to the full quantum theory. The most widely used of these is *Gross-Pitaevskii (GP) theory* — a mean-field theory which neglects quantum fluctuations entirely [9, 10].

In GP theory, the field operator $\hat{\Psi}(\mathbf{r}, t)$ which appears in the full quantum theory is replaced by a classical field $\Psi(\mathbf{r}, t)$, called the *mean-field order parameter* or *condensate wavefunction*. This replacement is valid only under certain conditions. In particular, the gas must be dilute so that interactions between atoms are weak, and it must be ultra-cold so that essentially all of the atoms are in the condensed state. Furthermore, the inter-atomic potential which appears in the full quantum theory, must be replaced by an effective pseudo-potential. This ensures that the mean-field (GP) theory reproduces the correct low-energy (s-wave) scattering properties.

Assuming these conditions have been met, the state of the BEC is well-described by the mean-field order parameter $\Psi(\mathbf{r}, t)$, which obeys the following partial integro-differential equation:

$$i\hbar \frac{\partial \Psi(\mathbf{r}, t)}{\partial t} = \left(-\frac{\hbar^2}{2M} \nabla^2 + V_{\text{ext}}(\mathbf{r}) + \int d\mathbf{r}' V(\mathbf{r} - \mathbf{r}') |\Psi(\mathbf{r}', t)|^2 \right) \Psi(\mathbf{r}, t). \quad (1.1)$$

This is the generalised GP equation for a Bose-condensed gas. Here, M denotes the mass of the atoms in the gas, $V_{\text{ext}}(\mathbf{r})$ denotes an external potential (e.g. a trapping potential), and $V(\mathbf{r})$ denotes the inter-atomic pseudo-potential. Owing to the similarities between this equation and the Schrödinger equation, it is common to regard the mean-field order parameter $\Psi(\mathbf{r}, t)$ as a wavefunction. One must be careful, however, not to confuse $\Psi(\mathbf{r}, t)$ with the many-body wavefunction of the gas. Instead, $\Psi(\mathbf{r}, t)$ should be interpreted as a single particle wavefunction which describes the state of each atom in the condensate. It is normalised so that $\int d\mathbf{r} |\Psi(\mathbf{r}, t)|^2 = N$, where N is the number of atoms in the condensed state.

Another useful result of the GP theory, is the GP energy functional:

$$E[\Psi] = \int d\mathbf{r} \left\{ \frac{\hbar^2}{2M} |\nabla \Psi(\mathbf{r}, t)|^2 + V_{\text{ext}}(\mathbf{r}) |\Psi(\mathbf{r}, t)|^2 \right\} + \frac{1}{2} \int d\mathbf{r} \int d\mathbf{r}' |\Psi(\mathbf{r}, t)|^2 V(\mathbf{r} - \mathbf{r}') |\Psi(\mathbf{r}', t)|^2, \quad (1.2)$$

which allows one to evaluate the energy of the condensate as a function of the mean-field order parameter. This is particularly useful in determining approximate analytic expressions for $\Psi(\mathbf{r}, t)$ by applying the variational principle.

1.3 Inter-atomic interactions

Many of the properties of BECs are governed by the interactions between the constituent atoms. In early experiments, researchers investigated dilute BECs formed from alkali metals, such as rubidium and sodium. In these BECs, the dominant interaction between atoms is a van-der-Waals-like interaction, which is isotropic and short-range, decaying as $\sim 1/r^6$. By considering this interaction rigorously using scattering theory, it is possible to show that s-wave collisions are dominant at low temperatures and particle number densities [11]. Higher-order partial wave collisions, such as p-wave and d-wave collisions, are suppressed. For the purposes of GP theory, this means that the van-der-Waals-like interaction may be effectively modelled using the following contact interaction pseudo-potential:

$$U_{\text{contact}}(\mathbf{r}) = g \delta(\mathbf{r}), \quad (1.3)$$

where $g = 4\pi\hbar^2 a_s/M$ and a_s is the s-wave scattering length. In experiments, the strength of the interaction, g , may be tuned over a wide range of values by applying an external magnetic field to the system. This exploits a phenomenon known as Feshbach resonance [12]. If g is tuned to be positive then the interaction between atoms is repulsive; if g is negative then the interaction is attractive.

By the early 2000s, BECs with contact interactions were quite well understood. As a result, researchers began to think about realising condensates with different, richer interactions. This led them to consider the *dipolar interaction*, which acts between particles with permanent electric or magnetic dipole moments. Unlike the contact interaction, the dipolar interaction is anisotropic and long-range, decaying as $\sim 1/r^3$. For the most general case in which the dipole moments are unpolarised (illustrated in Figure 1.1(a)), the form of the dipolar interaction potential is as follows:

$$U_{\text{dd}}(\mathbf{r}) = \frac{C_{\text{dd}}}{4\pi} \frac{(\hat{\mathbf{e}}_1 \cdot \hat{\mathbf{e}}_2) |\mathbf{r}|^2 - 3(\hat{\mathbf{e}}_1 \cdot \mathbf{r})(\hat{\mathbf{e}}_2 \cdot \mathbf{r})}{|\mathbf{r}|^5}. \quad (1.4)$$

Here $\hat{\mathbf{e}}_1$ and $\hat{\mathbf{e}}_2$ are unit vectors which specify the orientation of the dipole moments, \mathbf{r} is the relative separation of the particles, and C_{dd} is the coupling constant. If the particles have a permanent electric dipole moment, d , then $C_{\text{dd}} = d^2/\epsilon_0$; otherwise if the particles have a permanent magnetic dipole moment, μ , then $C_{\text{dd}} = \mu\mu_0$.

To date, the majority of research regarding the dipolar interaction in BECs has focussed on the special case in which the dipole moments are uniformly polarised by an external polarising field (see Figure 1.1(b)). In this case the anisotropy of the interaction is more pronounced (it tends to average out over a large number of particles in the un-polarised case). Assuming that the dipole moments are polarised along $\hat{\mathbf{p}}$, the dipolar interaction potential is given by:

$$U_{\text{dd}}(\mathbf{r}) = \frac{C_{\text{dd}}}{4\pi} \frac{1 - 3(\hat{\mathbf{p}} \cdot \hat{\mathbf{r}})^2}{|\mathbf{r}|^3}. \quad (1.5)$$

In this form, the anisotropy of the interaction is clear: as the angle between $\hat{\mathbf{p}}$ and $\hat{\mathbf{r}}$ changes, the numerator $1 - 3(\hat{\mathbf{p}} \cdot \hat{\mathbf{r}})^2$ varies between -2 and 1 . If the dipole moments sit side-by-side (see

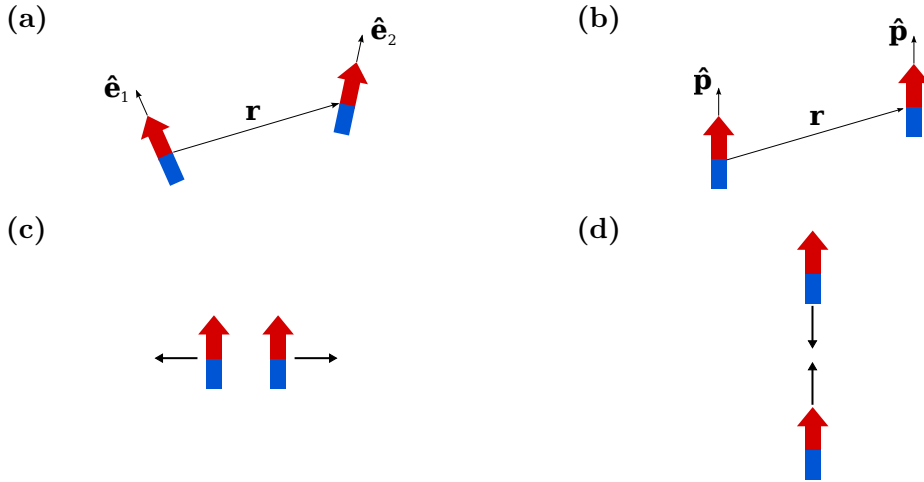


Figure 1.1: Two particles interacting via the dipolar interaction. (a) The un-polarised case. (b) The polarised case. (c) Dipoles oriented side-by-side feel a repulsive force. (d) Dipoles oriented top-to-tail feel an attractive force.

Figure 1.1(c)), then $\hat{\mathbf{p}} \cdot \hat{\mathbf{r}} = 0$ and the interaction is repulsive. However, if the dipole moments are in a top-to-tail configuration (see Figure 1.1(d)), then $\hat{\mathbf{p}} \cdot \hat{\mathbf{r}} = 1$ and the interaction is attractive.

In order to incorporate dipolar interactions into the GP theory, one must again derive an effective pseudo-potential to use in place of the true inter-atomic potential. By treating the problem rigorously using scattering theory [13, 14], one may show that the following pseudo-potential is appropriate away from scattering resonances:

$$V(\mathbf{r}) = U_{\text{contact}}(\mathbf{r}) + U_{\text{dd}}(\mathbf{r}), \quad (1.6)$$

where we note that the contact interaction strength g is now in principle a function of C_{dd} . This means that all partial waves contribute to scattering in the presence of dipolar interactions. As a result, both long-range and short-range interactions play a crucial role in the physics of dipolar BECs.

1.4 Superfluidity and vortices in BECs

A direct consequence of BEC in quantum gases is the phenomenon of *superfluidity*. In fact, it is possible to show, starting from the quantum field theory of BEC, that superfluidity arises from the way in which the field operator $\hat{\Psi}(\mathbf{r}, t)$ transforms between Galilean reference frames *and* the fact that a classical field $\Psi(\mathbf{r}, t)$ may be associated with the macroscopic component of $\hat{\Psi}(\mathbf{r}, t)$. Based on these considerations alone, one may deduce that the flow velocity of particles in a BEC is of the form:

$$\mathbf{v}(\mathbf{r}, t) = \frac{\hbar}{M} \nabla S(\mathbf{r}, t), \quad (1.7)$$

where $S(\mathbf{r}, t)$ is the phase of the classical field $\Psi(\mathbf{r}, t)$ [15]. With this result, it is clear that the flow velocity in a BEC must obey the irrotationality condition: $\nabla \times \mathbf{v} = 0$ — the hallmark of superfluidity.

As a result of the irrotationality of the flow velocity, BECs display a striking response to rotation. In an ordinary classic fluid rotating with angular velocity Ω , the flow velocity approaches that of a rotating rigid-body, such that $\nabla \times \mathbf{v} \rightarrow 2\Omega$. This classical fluid flow clearly violates the irrotationality condition of a superfluid. As a result, the only way in which a rotating BEC may acquire angular momentum, is through the nucleation of *quantised vortices*. These are singular points (in two dimensions) or lines (in three dimensions) of vanishing density, about which the circulation of $\mathbf{v}(\mathbf{r}, t)$ is quantised in units of h/M [15].

In general, quantised vortices are unstable configurations — they are only energetically favourable when the rotation frequency of the BEC exceeds a critical value Ω_c . The functional dependence of Ω_c has been investigated in trapped non-dipolar [16] and dipolar [17] BECs using a variational approach. Roughly speaking, one finds that the critical rotation frequency for vortex nucleation is of the same order as the radial trapping frequency ω_ρ . Typical values of Ω_c are between $0.3\omega_\rho$ and $0.9\omega_\rho$ — the exact value depends on the particular parameters of the system.

1.5 Vortex lattices

As the rotation frequency of a BEC is increased beyond the critical value Ω_c , more and more vortices will appear in the system as a means of storing angular momentum. If the rotation frequency is maintained at a fast, stable value, then the BEC will evolve to a state in which the vortices are arranged on the sites of a lattice (see Figure 1.2). In the rotating frame of reference, this vortex lattice state is stationary, implying that the lattice as a whole rotates as a rigid body at the same rotation frequency as the BEC.

Vortex lattices are not unique to rotating BECs — they are a general feature of rotating superfluids. In fact, the first studies of vortex lattices occurred in the 1950s and 1960s in the context of superconducting alloys and superfluid helium [18–20]. Russian physicist Abrikosov, made a number of important contributions to these studies: in particular, he predicted that the geometry of the lattice would be triangular [19]. This was confirmed experimentally for the first time in superconducting niobium in 1964 [20].

In the late 1990s, the study of vortex lattices was revived in the context of BECs. A significant amount of research has already been conducted in this area, with researchers considering equilibrium properties, such as lattice geometry [21, 22] and lattice uniformity [23, 24], as well as non-equilibrium properties, such as Tkachenko waves [25, 26] and vortex aggregation [27]. However, much of the work thus far has focussed on vortex lattices in non-dipolar BECs. Whilst there have been a few theoretical studies in the dipolar case [1, 2, 28], these studies have not yet been supported by experiment.

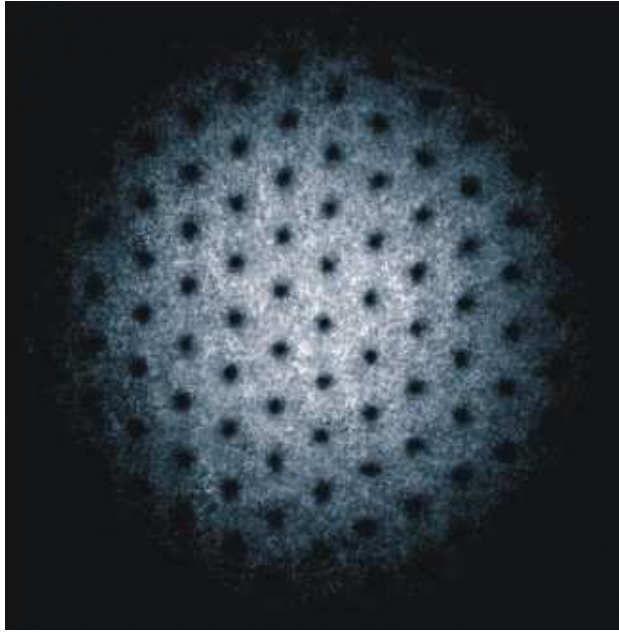


Figure 1.2: Experimentally-obtained image of a triangular vortex lattice in a rapidly-rotating condensate of ^{87}Rb atoms. (Source: Coddington et al. *Phys. Rev. A.* **70** 063607)

1.6 A new research problem

In this thesis, I will develop a method for analysing vortex lattice geometry in fast-rotating dipolar BECs. This problem has already been covered rather extensively for the case of non-dipolar BECs, where it is known from theory [21, 29] and experiment [30] that the lattice geometry is always triangular. A few theoretical studies have also been conducted for the dipolar case which show that non-triangular lattice geometries are possible [1, 2, 28], however they are restricted to a special situation in which the dipole polarisation is fixed along the rotation axis. In addition, these previous studies also use different analytic methods to the one I shall use here.

In Zhang and Zhai's study, the dipolar interaction potential is assumed to be strictly two-dimensional, rather than a more realistic quasi-two-dimensional potential [1]. Their treatment of the problem is otherwise quite similar to my own, excluding the fact that their treatment is limited to the special case of on-axis polarisation. Cooper et al. take a very different analytic approach compared to that of Zhang and Zhai and my own. They discretise space and consider a small region of the BEC subject to periodic boundary conditions, rather than considering the vortex lattice over the entire BEC [2]. Yi and Pu approach the problem in a completely different way, by numerically simulating the GP equation [28]. This approach should theoretically give the most accurate results, however it is difficult to systematically cover the entire parameter space in this way, because it is necessary to run an enormous number of simulations.

In developing my own method of studying vortex lattices in dipolar BECs, I shall draw on a method that was originally used in the study of vortex lattices in two-component non-dipolar BECs due to Mueller and Ho [31]. Building on this method, I aim to investigate vortex

lattice geometry in fast-rotating, trapped dipolar BECs for arbitrary relative interaction strength $\epsilon_{\text{dd}} = C_{\text{dd}}/3g$ and arbitrary dipole polarisation $\hat{\mathbf{p}}$. In doing so, I shall make the following assumptions:

- *fast rotation*: the rotation frequency of the gas, Ω , approaches the transverse trapping frequency ω_ρ ,
- *weak interactions*: the mean interaction energy per atom is much smaller than the trap energies $\hbar\omega_\rho$ and $\hbar\omega_z$,
- *centred uniform lattice*: the vortices are arranged on a lattice which is not deformed, with one of the vortices centred on the axis of rotation.

Chapter 2

Vortex lattices in non-dipolar BECs

We shall begin our analysis by considering vortex lattices for the simplest case of a non-dipolar BEC. Although this case has been covered rather extensively in the literature, it will be useful for the reader to provide a comprehensive, self-contained review here. In later chapters, we shall build on the results and methodology presented in this review to extend our analysis to the dipolar case. By neglecting dipolar interactions for now, we may avoid a great deal of convoluted mathematics which only serves as a distraction to the reader at this point.

Our method for analysing vortex lattices will essentially be an application of the variational principle, which is covered in most elementary quantum mechanics texts. A basic outline of the method is as follows:

1. Make an ansatz for the condensate wavefunction which describes an arbitrary vortex lattice as a function of various parameters.
2. Substitute the ansatz for the condensate wavefunction into the energy functional.
3. Minimise the energy with respect to the parameters which describe the lattice in order to obtain the “optimal” vortex lattice solution.

Although this seems quite straightforward, each step requires us to deal with a number of intricacies. Step 1 in particular is highly non-trivial, because we must somehow make an appropriate guess for the form of the condensate wavefunction, which at the same time, is flexible enough to describe all possible types of vortex lattice. To guide us along these lines, we shall begin by considering the form of the energy functional (and Hamiltonian) for the system.

2.1 The energy functional for a rotating BEC in quasi-2D

We have already seen an expression for the energy functional of a condensate in Section 1.2. Whilst this expression is quite general, it is not useful for our study of vortex lattices because

it requires that the condensate be in a stationary state. This is not physically possible when vortices are present, because the condensate must be rotating in order for vortices to appear, and the rotation breaks the time-independence of the Hamiltonian. Our focus in this section will therefore be to derive an alternative expression for the energy which is applicable to rotating condensates.

In order to proceed, we transform to a reference frame in which the condensate appears to be in a stationary state. Until now, we have been working in the laboratory frame. An observer in the laboratory frame will see the condensate rotating at the same frequency as the external potential which is driving the rotation. To make the condensate appear stationary, we must therefore transform to a frame that rotates along with the external driving potential. The Hamiltonian in this new rotating frame is given by $H' = H - \mathbf{L} \cdot \boldsymbol{\Omega}$ where H is the Hamiltonian for the non-rotating system, \mathbf{L} is the angular momentum operator and $\boldsymbol{\Omega}$ is the angular velocity of the rotation [32]. In the rotating frame, it now makes sense to look for stationary solutions because H' is time-independent. This means we can use the expression for the energy functional given in Equation (1.2) so long as we work in the rotating frame.

Let us now evaluate the energy functional in the rotating frame for the specific system we would like to consider. We shall assume that the condensate is comprised of N identical bosonic particles of mass M , and that it is rotating at constant angular velocity Ω about the z -axis. Furthermore, we shall assume that the condensate is confined in a cylindrically symmetric harmonic trap with longitudinal and radial trap frequencies denoted by ω_z and ω_ρ respectively. Using the theory of Section 1.2 as a reference, we have that the energy functional in the rotating frame is given by

$$E'[\Psi] = \underbrace{\int d\mathbf{r} \Psi(\mathbf{r})^* H'_0 \Psi(\mathbf{r})}_{E'_0[\Psi]} + \underbrace{\frac{1}{2} \int d\mathbf{r}_1 \int d\mathbf{r}_2 \varrho(\mathbf{r}_1) V(\mathbf{r}_1 - \mathbf{r}_2) \varrho(\mathbf{r}_2)}_{E_{\text{int}}[\Psi]}, \quad (2.1)$$

where $\varrho(\mathbf{r}) = |\Psi(\mathbf{r})|^2$ is defined to be the condensate density. There are two distinct contributions to the total energy: a single-particle energy contribution E'_0 , and an interaction energy contribution E_{int} . The single-particle energy contribution is associated with the Hamiltonian

$$H'_0 = \frac{1}{2M} (\mathbf{i}\hbar\nabla + \Omega M \hat{\mathbf{z}} \times \boldsymbol{\rho})^2 + \frac{1}{2} M (\omega_\rho^2 - \Omega^2) \boldsymbol{\rho}^2 + \frac{1}{2} M \omega_z^2 z^2. \quad (2.2)$$

This includes the kinetic energy term and the external trapping potential, both of which appear slightly modified due to the presence of rotation (recall that $H'_0 = H_0 - \Omega L_z$). The interaction energy contribution is associated with the two-particle pseudo-potential

$$V(\mathbf{r}) = g \delta(\mathbf{r}). \quad (2.3)$$

Only contact interactions are included here since we are considering the non-dipolar case.

With Equation (2.1), we have achieved our goal of finding an expression for the energy of a rotating condensate. However, we can reduce this expression further if we assume that the condensate is in the quasi-two-dimensional (quasi-2D) regime. In this regime, the

condensate cloud is flattened out like a pancake (extremely oblate) and the z degree of freedom is effectively frozen. Physically, this corresponds to a situation where the condensate is rapidly rotating so that centrifugal spreading is significant, and where the longitudinal trapping is strong ($\hbar\omega_z \gg g\varrho(0)$) [33]. In such circumstances it is appropriate to assume that the longitudinal motion is described by the ground state of the z -confinement, so that the condensate wavefunction is of the form

$$\Psi(\mathbf{r}) = \frac{1}{(\pi l_z^2)^{\frac{1}{4}}} \exp\left(-\frac{z^2}{2l_z^2}\right) \Phi(\boldsymbol{\rho}), \quad (2.4)$$

where $l_z = \sqrt{\hbar/M\omega_z}$ is the longitudinal harmonic oscillator length.¹ With this prescription for $\Psi(\mathbf{r})$ we have defined a two-dimensional condensate wavefunction $\Phi(\boldsymbol{\rho})$, which only depends on the coordinates in the rotating plane $\boldsymbol{\rho} = (x, y)$. To ensure that the total particle number constraint continues to be satisfied, the two-dimensional condensate density $n(\boldsymbol{\rho}) = |\Phi(\boldsymbol{\rho})|^2$ must be normalised so that $\int d\boldsymbol{\rho} n(\boldsymbol{\rho}) = N$.

Using this ansatz for $\Psi(\mathbf{r})$ we may recast the expression for the condensate energy in quasi-2D. Substituting Equation (2.4) into Equation (2.1) and integrating over z , we obtain

$$E_0[\Phi] = \frac{1}{2}N\hbar\omega_z + \int d\boldsymbol{\rho} \Phi(\boldsymbol{\rho})^* \bar{H}'_0 \Phi(\boldsymbol{\rho}) \quad (2.5)$$

for the single particle energy contribution, with an effective two-dimensional single-particle Hamiltonian given by

$$\bar{H}'_0 = -\frac{1}{2M}(\mathrm{i}\hbar\nabla_{\perp} + \Omega M\hat{\mathbf{z}} \times \boldsymbol{\rho})^2 + \frac{1}{2}M(\omega_{\rho}^2 - \Omega^2)\boldsymbol{\rho}^2. \quad (2.6)$$

Similarly, for the interaction energy contribution we obtain:

$$E_{\mathrm{int}}[\Phi] = \frac{1}{2}g_{2\mathrm{D}} \int d\boldsymbol{\rho} n(\boldsymbol{\rho})^2, \quad (2.7)$$

where we have introduced a modified two-dimensional coupling strength $g_{2\mathrm{D}} = g/\sqrt{2\pi}l_z$.

The next step in the vortex lattice analysis is to make some assumptions about the form of $\Phi(\boldsymbol{\rho})$ so that we may further reduce Equations (2.5) and (2.7) above. We shall consider these assumptions in detail in the following section.

2.2 Ansatz for the vortex lattice ground state

Thus far we have not made any specifications about vortices in the condensate. In this section, we shall develop an ansatz for the two-dimensional ground state condensate wavefunction which assumes that vortices exist on the sites of a lattice. To make the problem analytically tractable we must rely on three assumptions: firstly that the condensate is in the fast-rotating

¹See [34] for a semi-rigorous justification based on a multiple-scale analysis of the GP equation.

limit, secondly that the interactions are relatively weak, and thirdly that the vortex lattice is regular and infinite in extent (see Section 1.6).

2.2.1 The lowest Landau level (LLL) state and a link to vortices

We begin by considering the fast-rotating limit where $\Omega \rightarrow \omega_\rho$. This is the point at which the centrifugal spreading due to rotation almost overwhelms the confinement due to the radial trap. In this limit, the single-particle Hamiltonian in quasi-2D tends to $-(i\hbar\nabla_\perp + \Omega M\hat{\mathbf{z}} \times \boldsymbol{\rho})^2/2M$, up to a constant. The eigenfunctions of this Hamiltonian are well known: they are the Landau level orbitals $u_{m,n}(x, y)$ with corresponding eigenenergies $\epsilon_n = \hbar\Omega(n + 1/2)$. The n quantum number labels the so-called *Landau level*, and may take on any non-negative integer value. Each Landau level is infinitely degenerate since ϵ_n does not depend on m (which also takes on non-negative integer values).

Although the Landau level orbitals do not necessarily form a complete basis for the full quasi-2D Hamiltonian $\bar{H}'_0 + \bar{V}$, if we assume that the interactions are weak then they are a good approximate basis choice [35]. In searching for the ground state of the condensate, we shall therefore assume that it is adequately described by a superposition of $n = 0$ Landau level orbitals. This is called a lowest Landau level (LLL) state. Consequently, we may write the two-dimensional ground state wavefunction of the condensate as:

$$\Phi(\boldsymbol{\rho}) = \sum_{m=0}^{\infty} c_m u_{m,0}(\boldsymbol{\rho}) = \sum_{m=0}^{\infty} \frac{c_m}{\sqrt{2\pi m!}} \left(\frac{x + iy}{l_\rho} \right)^m \exp\left(-\frac{x^2 + y^2}{2l_\rho^2}\right), \quad (2.8)$$

where the right-hand side follows from the explicit form of $u_{m,0}(x, y)$. The length scale $l_\rho = \sqrt{\hbar/M\Omega}$ is effectively equal to the transverse trap length since $\Omega \rightarrow \omega_\rho$.

At this point it turns out to be convenient to convert to a complex number representation, rather than working with the components of a two-dimensional vector. To this end, we map $\boldsymbol{\rho} = x\hat{\mathbf{x}} + y\hat{\mathbf{y}}$ to the complex number $w = x + iy$. In the complex number representation, the ground state wavefunction of Equation (2.8) may be written as

$$\Phi(w) = f(w) \exp\left(-\frac{|w|^2}{2l_\rho^2}\right) \quad (2.9)$$

where f is an analytic function of w . With this definition, the coefficients of the superposition c_m have been absorbed into f . This is not an issue however, because we shall never need to work with these coefficients directly. Instead, we may fully specify f in terms of its roots since it is an analytic function. In fact, it is possible to show that each root specifies the location of a vortex core at the corresponding x and y coordinates in the condensate [31]. Thus we may alternatively specify the ground state by giving the locations of all of the vortex cores.

With this realisation, it is clear that a vortex lattice ground state corresponds to a situation where the roots of f lie on a lattice. Our next step will therefore be to construct an analytic function with roots that satisfy this property. Fortunately, there is a well-studied function in

complex analysis which will be useful here: the Jacobi theta function $\theta_1(z, \varsigma)$. The roots of $\theta_1(z, \varsigma)$ are able to describe any regular lattice up to a rotation by making an appropriate choice for the parameter ς . This means that f may be expressed in terms of θ_1 to obtain a vortex lattice ground state wavefunction. However in order to make this connection, we must first introduce a way to describe the lattice mathematically.

2.2.2 Mathematical description of the vortex lattice

A two-dimensional lattice may be fully specified by a pair of basis vectors: \mathbf{b}_1 and \mathbf{b}_2 . The points of the lattice are obtained from these basis vectors by constructing all possible linear combinations of the form $m_1\mathbf{b}_1 + m_2\mathbf{b}_2$ where m_1 and m_2 are integers. Each one of these linear combinations is called a *lattice vector*.

In general, four real parameters are required to fully specify a lattice: two real components for each of the two basis vectors. However for our current purposes one of these parameters may be fixed, since we shall not distinguish between lattices which are equivalent up to a rotation. This is justified because the Hamiltonian which describes the non-dipolar condensate is cylindrically symmetric. In order to fix one of the parameters, we shall choose to orient the first basis vector \mathbf{b}_1 along the x -axis. This choice of orientation will turn out to be convenient later on in making a connection with the roots of the Jacobi theta function.

The three remaining parameters we shall use to describe the lattice are depicted in Figure 2.1, along with the lattice basis vectors. The first basis vector \mathbf{b}_1 is specified solely in terms of its magnitude, which is denoted by the parameter b_1 , since its direction is fixed along $\hat{\mathbf{x}}$. The second basis vector \mathbf{b}_2 is defined with reference to the first basis vector through a rotation and rescaling. This requires two additional parameters: a rotation angle η and a scaling factor τ . Writing out the basis vectors explicitly in terms of the parameters b_1 , τ and η , we have that $\mathbf{b}_1 = b_1\hat{\mathbf{x}}$ and $\mathbf{b}_2 = \tau b_1(\cos \eta \hat{\mathbf{x}} + \sin \eta \hat{\mathbf{y}})$.

The other parameter that appears in Figure 2.1 is the area of the unit cell, given by $v_c = b_1^2\tau \sin \eta$. This parameter is redundant in specifying the lattice because it depends on the other parameters: b_1 , τ and η . However, it is useful to mention it because it appears in a number of places in the subsequent analysis.

Another useful concept regarding our mathematical description of the vortex lattice is the *reciprocal lattice*. It is needed to represent a function which is defined on a lattice as a Fourier series. The reciprocal lattice is obtained from the original lattice by a transformation of the lattice basis vectors. We shall denote the basis vectors of the reciprocal lattice as \mathbf{q}_1 and \mathbf{q}_2 . They are obtained from \mathbf{b}_1 and \mathbf{b}_2 as follows: $\mathbf{q}_1 = \frac{2\pi}{v_c}\mathbf{b}_2 \times \hat{\mathbf{z}} = \frac{2\pi b_1 \tau}{v_c}(\sin \eta \hat{\mathbf{x}} - \cos \eta \hat{\mathbf{y}})$ and $\mathbf{q}_2 = \frac{2\pi}{v_c}\hat{\mathbf{z}} \times \mathbf{b}_1 = \frac{2\pi b_1}{v_c}\hat{\mathbf{y}}$. As for the case of the original lattice, the reciprocal lattice is constructed from its basis vectors by considering all linear combinations of the form $m_1\mathbf{q}_1 + m_2\mathbf{q}_2$ where m_1 and m_2 are integers. Each one of these linear combinations is called a *reciprocal lattice vector*, which we shall denote in general by \mathbf{q} .

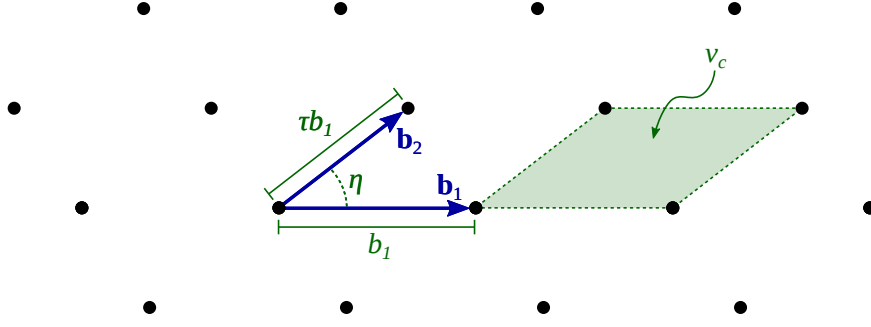


Figure 2.1: Illustration of the lattice basis vectors and the lattice parameters.

2.2.3 Derivation of the vortex lattice ground state

Now that we have a way to describe lattices mathematically, we can continue the derivation of the vortex lattice ground state. We previously indicated that it would be possible to map the points of the vortex lattice (or equivalently the roots of f) onto the roots of the Jacobi theta function. In the language we have just developed, the roots of the Jacobi theta function $\theta_1(z, \varsigma)$ correspond to a lattice with $b_1 = 1$ and $\varsigma = e^{i\pi\tau e^{i\eta}}$. This would describe an arbitrary lattice, if the magnitude of the first basis vector b_1 were not fixed to unity. To reintroduce an arbitrary magnitude, we divide the first argument of θ_1 by b_1 . Then f may be expressed in terms of θ_1 by writing

$$f(w) = C^{\frac{1}{2}} h(w/b_1) \theta_1(w/b_1, \varsigma), \quad (2.10)$$

where h is an entire function without any roots and C is a normalisation factor. Putting this into Equation (2.9) yields the following expression for the two-dimensional condensate density:

$$n(\boldsymbol{\rho}) = C |h(w/b_1)|^2 |\theta_1(w/b_1, \varsigma)|^2 \exp\left(-\frac{|w|^2}{l_\rho^2}\right). \quad (2.11)$$

Motivated by the fact that the roots of $|\theta_1(w/b_1, \varsigma)|^2$ lie on a lattice, we shall attempt to express this function as a Fourier series. Using the Laurent series definition of θ_1 , it is possible to show, after substantial manipulation, that

$$|\theta_1(w/b_1, \varsigma)|^2 = e^{2\pi y^2/v_c} \sum_{\mathbf{q}} g_{\mathbf{q}} e^{i\mathbf{q}\cdot\boldsymbol{\rho}}; \quad g_{\mathbf{q}} = \frac{(-1)^{m_1+m_2} e^{-v_c \mathbf{q}^2/8\pi}}{\sqrt{\tau} \sin \eta}. \quad (2.12)$$

The factor $\sum_{\mathbf{q}} g_{\mathbf{q}} e^{i\mathbf{q}\cdot\boldsymbol{\rho}}$ is a Fourier series defined on the vortex lattice. Here we are using a shorthand notation in which a sum over \mathbf{q} represents a sum over all of the reciprocal lattice vectors. In keeping with the notation used previously, a particular reciprocal lattice vector is denoted by $\mathbf{q} = m_1 \mathbf{q}_1 + m_2 \mathbf{q}_2$. This means that the sum over \mathbf{q} is really a sum over the integers m_1 and m_2 .

The final key step in the derivation is to make use of the cylindrical symmetry of the condensate cloud. We know that the condensate cloud must be cylindrically symmetric because the Hamiltonian has cylindrical symmetry. Enforcing this condition, it is possible to show that $h(w) = \exp(\pi w^2/2\tau \sin \eta)$.

Combining these results and performing normalisation, we finally have that

$$n(\boldsymbol{\rho}) = \frac{N}{\pi\sigma^2} e^{-\frac{\rho^2}{\sigma^2}} g(\boldsymbol{\rho}). \quad (2.13)$$

In other words, the two-dimensional condensate density is the product of a Gaussian envelope and a function $g(\boldsymbol{\rho}) = \sum_{\mathbf{q}} \bar{g}_{\mathbf{q}} e^{i\mathbf{q}\cdot\boldsymbol{\rho}}$ which is periodic on the vortex lattice. The Fourier coefficients of $g(\boldsymbol{\rho})$ are rescaled compared to those derived in Equation (2.12) so that $\bar{g}_{\mathbf{q}} = g_{\mathbf{q}} / \sum_{\mathbf{v}} g_{\mathbf{v}} e^{-\frac{\sigma^2 \mathbf{v}^2}{4}}$. The radial extent of the condensate cloud is quantified by the length-scale $\sigma = (l_{\rho}^{-2} - \pi v_c^{-1})^{-1/2}$ which is related to the number of vortices in the system.

2.3 Evaluation of the energy in the vortex lattice ground state

Now that we have an ansatz for the vortex lattice ground state, we can finally calculate the energy of the condensate as a function of the lattice parameters. Using the fact that $\Phi(\boldsymbol{\rho})$ is in the LLL, the single-particle energy contribution simplifies to

$$E_0[n] = N(\hbar\Omega + \frac{1}{2}\hbar\omega_z) + \frac{\hbar(\omega_{\rho}^2 - \Omega^2)}{2\Omega l_{\rho}^2} \langle \boldsymbol{\rho}^2 \rangle \quad (2.14)$$

where $\langle \boldsymbol{\rho}^2 \rangle \equiv \int d\boldsymbol{\rho} \boldsymbol{\rho}^2 n(\boldsymbol{\rho})$. Substituting the explicit expression for $n(\boldsymbol{\rho})$ from Equation (2.13), we find that

$$\langle \boldsymbol{\rho}^2 \rangle = N\sigma^2 \sum_{\mathbf{q}} \bar{g}_{\mathbf{q}} e^{-\frac{\sigma^2 \mathbf{q}^2}{4}} \left(1 - \frac{\sigma^2 \mathbf{q}^2}{4} \right) \approx N\sigma^2,$$

where the approximate result follows in the limit of large vortex number: $\sigma^2 \mathbf{q}^2 \gg 1$. In this limit, the single-particle energy contribution is therefore independent of the lattice parameters.

Next we evaluate the interaction energy contribution, which from Equation (2.7), may be rewritten in the following form:

$$E_{\text{int}}[n] = \frac{N^2 g_{2D}}{2\pi\sigma^2} \mathcal{I}[n]. \quad (2.15)$$

Here we have defined $\mathcal{I}[n] \equiv (\pi\sigma^2/N^2) \int d\boldsymbol{\rho} n(\boldsymbol{\rho})^2$; a dimensionless analogue of the interaction energy contribution. Substituting the ansatz for the vortex lattice ground state from

Equation (2.13), we find that

$$\mathcal{I}(\tau, \eta) = \frac{1}{2} \sum_{\mathbf{q}, \mathbf{v}} \bar{g}_{\mathbf{q}} \bar{g}_{\mathbf{v}} e^{-\frac{\sigma^2 |\mathbf{q} + \mathbf{v}|^2}{8}}. \quad (2.16)$$

This quantity depends on τ and η implicitly through its dependence on the reciprocal lattice vectors. If we again consider the limit of large vortex number where $\sigma^2 \mathbf{q}^2 \gg 1$, it is possible to simplify this expression quite significantly. In fact, one may assume that the exponential factor $e^{-\frac{\sigma^2 |\mathbf{q} + \mathbf{v}|^2}{8}}$ is so sharply peaked at $\mathbf{q} = -\mathbf{v}$ that it may be approximated by a Kronecker delta: $\delta_{\mathbf{q}, -\mathbf{v}}$. This collapses the double sum over \mathbf{q} and \mathbf{v} to a single sum over \mathbf{q} , which is much simpler to evaluate:

$$\begin{aligned} \mathcal{I}(\tau, \eta) &\approx \frac{1}{2} \sum_{\mathbf{q}} (\bar{g}_{\mathbf{q}})^2 \\ &= \sum_{m_1, m_2 = -\infty}^{\infty} \frac{1}{2} \exp \left[\pi \left(2m_1 m_2 \cot \eta - m_1^2 \tau \csc \eta - \frac{m_2^2 \csc \eta}{\tau} \right) \right]. \end{aligned} \quad (2.17)$$

With these results, we now have an expression for the total condensate energy $E(\tau, \eta) = E_0 + E_{\text{int}}(\tau, \eta)$ in the vortex lattice ground state as a function of the lattice parameters τ and η . In the following section, we shall use these results to minimise $E(\tau, \eta)$ and thereby determine the optimal vortex lattice geometry.

2.4 Optimal vortex lattice geometry

Until now, our efforts have been focussed on completing the first two steps of the variational method: developing an ansatz for the vortex lattice ground state, and substituting it into the energy functional. In this section we shall complete the final step: minimisation of the energy with respect to the variational parameters τ and η .

To begin, we note that only the interaction energy contribution depends on τ and η ; the single-particle energy contribution is effectively a constant. Consequently, we may minimise the total energy $E(\tau, \eta) = E_0 + E_{\text{int}}(\tau, \eta)$ with respect to τ and η by minimising $E_{\text{int}}(\tau, \eta)$ alone. Recalling the definition of $E_{\text{int}}(\tau, \eta)$ given in Equation (2.15), we see that minimisation of $E_{\text{int}}(\tau, \eta)$ is equivalent to minimisation of $\mathcal{I}(\tau, \eta)$ so long as the constant of proportionality $N^2 g_{2D} / 2\pi\sigma^2$ is positive. We may safely assume that this is the case because a negative constant of proportionality implies that g is negative, and this corresponds to a situation where the condensate is highly susceptible to collapse [36].

In order to minimise $\mathcal{I}(\tau, \eta)$ as defined in Equation (2.17), we must resort to a numerical treatment. This requires that we cut off the sums over m_1 and m_2 at some upper and lower bound. Here we shall choose the upper and lower bounds to be at $+M$ and $-M$ respectively, with M set to 15. This ensures that $\mathcal{I}(\tau, \eta)$ is accurate to machine precision for values of τ and η greater than about 0.05. If we wanted to explore regions in which τ or η is less than

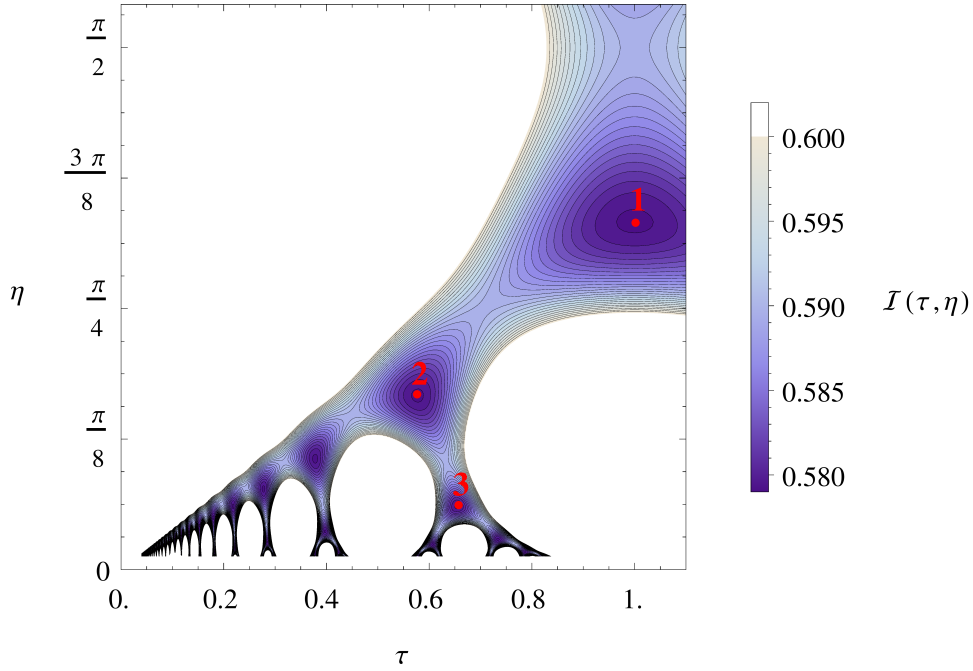


Figure 2.2: Contour plot of $\mathcal{I}(\tau, \eta)$ — a dimensionless analogue of the interaction energy. The white areas are regions where $\mathcal{I}(\tau, \eta)$ is greater than the cut-off value of 0.6. The purple areas correspond to regions where $\mathcal{I}(\tau, \eta)$ approaches its minimum value. Multiple local minima are visible, although they become difficult to see in the lower left-hand region of the plot. The three minima labelled by red numbers are mentioned in the text.

0.05, we would need to increase M above 15 to include higher frequency terms in the Fourier series. Fortunately, we can reasonably exclude these regions from our analysis because they correspond to an unphysical situation where the vortex lattice begins to collapse onto a line.

It is illustrative to perform the minimisation of $\mathcal{I}(\tau, \eta)$ graphically, by generating a contour plot of $\mathcal{I}(\tau, \eta)$ as a function of τ and η . The result is shown in Figure 2.2. In this plot, the dark purple shading corresponds to regions where $\mathcal{I}(\tau, \eta)$ approaches its minimum value. The white areas correspond to regions where $\mathcal{I}(\tau, \eta)$ is greater than the cut-off value, which is in this case set to 0.6. We have chosen to cut off the plot at this value to focus on the details around the minima and to avoid capturing regions where $\mathcal{I}(\tau, \eta)$ diverges.

Looking at Figure 2.2, we see that there are multiple local minima in the region plotted. A small selection of these minima are labelled by red numbers. Their (τ, η) coordinates are as follows:

$$\begin{aligned}
 1 : & \quad (1.0000\dots, 1.0472\dots) = \left(1, \frac{\pi}{3}\right) \\
 2 : & \quad (0.5773\dots, 0.5235\dots) = \left(\frac{1}{\sqrt{3}}, \frac{\pi}{6}\right) \\
 3 : & \quad (0.6546\dots, 0.1901\dots) = \left(\frac{\sqrt{3}}{\sqrt{7}}, \arcsin\left(\frac{\sqrt{3}}{\sqrt{7}}\right) - \frac{\pi}{6}\right) \\
 & \quad \vdots \quad \text{etc.}
 \end{aligned}$$

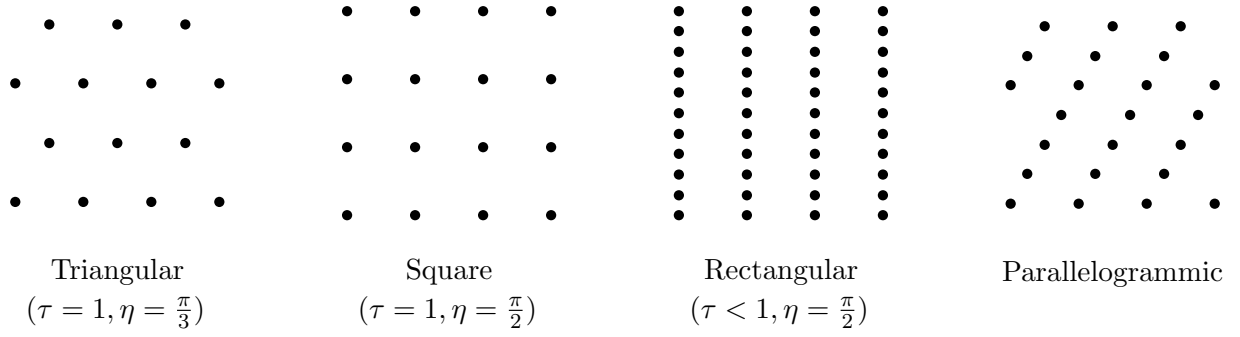


Figure 2.3: A lattice may be classified as one of four types according to the geometry of the unit cell. The triangular, square and rectangular lattices are all special cases of the parallelogrammic lattice. For the triangular, square and rectangular lattice, we have given the corresponding (τ, η) values in the so-called *standard parametrisation*. The (τ, η) values are omitted for the parallelogrammic lattice because they are not easily specified.

Since we would like to determine the *global* minimum, we should check all of the local minima to determine which has the smallest value. Performing this check numerically, we find that each local minimum has the same value of \mathcal{I} equal to $0.5797\dots$. It would therefore appear that there are multiple valid solutions to the minimisation problem! However upon more careful consideration, we may show that each of these solutions in fact corresponds to the same type of lattice; just at a different scale and orientation.

The solution labelled ‘1’ in the list above is what we shall call the *standard parametrisation* of the triangular lattice. It is illustrated in Figure 2.3, along with the standard parametrisations of the three other types of lattice: square, rectangular and parallelogrammic. In general, the standard parametrisation is defined to be the one for which τ is closest to 1. Alternative parametrisations of the same lattice have smaller values of τ compared to the standard one, and correspond to trivial rotations and rescalings of the lattice. For example, the second solution in the list above is an equally valid parametrisation of the triangular lattice. It can be obtained from the standard parametrisation $(\tau, \eta) = (1, \frac{\pi}{3})$ by applying the following transformation:

1. Choose an alternative pair of basis vectors: $\mathbf{b}'_1 = \mathbf{b}_1$ and $\mathbf{b}'_2 = \mathbf{b}_1 + \mathbf{b}_2$.
2. Rotate and rescale the alternative basis vectors so that \mathbf{b}'_2 is mapped to $\hat{\mathbf{x}}$. This means we must rotate clockwise through an angle of $\frac{\pi}{6}$ and rescale by $\frac{1}{\sqrt{3}}$.
3. Calculate the new lattice parameters from the transformed basis vectors. We find that $\tau = \frac{1}{\sqrt{3}}$ and $\eta = \frac{\pi}{6}$, which proves that solution 2 is related to the standard parametrisation (solution 1) by a trivial transformation.

By repeating this procedure with different combinations of basis vectors, we may relate all of the solutions seen in Figure 2.2 to the standard parametrisation of the triangular lattice. Hence we conclude that a triangular vortex lattice geometry is favoured in non-dipolar BECs.²

²A visualisation of the condensate density for the triangular lattice geometry is shown on the front cover of this thesis (top-left circle).

2.5 Summary

We have verified that a triangular vortex lattice geometry is always favoured in non-dipolar BECs using our variational method. Of course, this was to be expected based on the results of numerous experiments and previous theoretical studies, as referenced in Section 1.5. It is interesting to note, however, that the triangular lattice geometry is not significantly favoured over other possible lattice geometries. In particular, the energy corresponding to the square lattice geometry at $\tau = 1, \eta = \frac{\pi}{2}$ (which is a saddle point in Figure 2.2) is only 1.8% larger than that of the triangular lattice geometry. It is therefore conceivable that the energy minimum may shift to a non-triangular lattice geometry if the functional form of the interaction energy contribution is somehow altered. In order to explore this idea further, it will be interesting to investigate vortex lattices in BECs with different (i.e. non-contact) interactions. We shall begin along this path in the next chapter, by extending our analysis to consider vortex lattices in dipolar BECs.

Chapter 3

Vortex lattices in dipolar BECs with on-axis polarisation

In the previous chapter, we showed using a variational approach, that triangular vortex lattices are always favoured in non-dipolar BECs. It is not possible to observe other vortex lattice geometries, at least over the range of parameters that satisfy our assumptions. In this respect, non-dipolar BECs are not particularly interesting. In this chapter, we shall therefore turn our attention to dipolar BECs, in the hope that they may be able to support other vortex lattice geometries, such as square, rectangular and parallelogrammic. For now, we shall confine our attention to a specific class of dipolar BECs in which the dipoles are aligned along the axis of rotation — the z -axis for our choice of coordinate system. This is the so-called case of *on-axis polarisation*. Once we incorporate the effect of the dipoles into our theoretical description of the BEC, the vortex lattice analysis will proceed in much the same way as for the non-dipolar case. In fact, we shall refer to a number of results from the previous chapter to avoid duplication of work.

3.1 Modifying the two-particle pseudo-potential

When we considered non-dipolar BECs in the previous chapter, the two-particle pseudo-potential was simply equal to the contact interaction potential, $U_{\text{cont}}(\mathbf{r})$. However for the case of dipolar BECs, we must modify the two-particle pseudo-potential to include the dipolar interaction potential, $U_{\text{dd}}(\mathbf{r})$, so that

$$V(\mathbf{r}) = U_{\text{cont}}(\mathbf{r}) + U_{\text{dd}}(\mathbf{r}). \quad (3.1)$$

This is the only modification to the theory that is required to account for the effect of the dipoles.

In this chapter, $U_{\text{dd}}(\mathbf{r})$ adopts a simpler form compared to that of Equation (1.5), since we are assuming on-axis polarisation. Setting $\hat{\mathbf{p}} = \hat{\mathbf{z}}$, we find that

$$U_{\text{dd}}(\mathbf{r}) = \frac{C_{\text{dd}}}{4\pi} \frac{1 - 3 \cos^2 \theta}{r^3}, \quad (3.2)$$

where the vector \mathbf{r} is expressed here in spherical coordinates (r, θ, ϕ) . It is interesting to note that this expression does not depend on the azimuthal angle ϕ . This implies that the cylindrical symmetry of the Hamiltonian $H'_0 + V$ is maintained.

As a consequence of including $U_{\text{dd}}(\mathbf{r})$ in the two-particle pseudo-potential, we now have an additional contribution to the energy functional which was defined generally in Equation (2.1). This additional contribution is given by

$$E_{\text{dd}}[\Psi] = \frac{1}{2} \int d\mathbf{r}_1 \int d\mathbf{r}_2 \varrho(\mathbf{r}_1) U_{\text{dd}}(\mathbf{r}_1 - \mathbf{r}_2) \varrho(\mathbf{r}_2), \quad (3.3)$$

which we shall call the *dipolar interaction energy contribution*. Adding this to the single-particle and contact interaction energy contributions defined in Equations (2.1) and (2.14) respectively, gives the total energy in the rotating frame for a dipolar BEC:

$$E'[\Psi] = E'_0[\Psi] + E_{\text{cont}}[\Psi] + E_{\text{dd}}[\Psi]. \quad (3.4)$$

With this result, we may now embark on the vortex lattice analysis. Recalling the procedure established for the non-dipolar case, our first task will be to evaluate the condensate energy given above in the quasi-2D vortex lattice ground state. Since the single-particle and contact interaction energy contributions are unchanged from the non-dipolar case, we may use the expressions for them derived in Chapter 2. All that remains then, is to perform the calculation for $E_{\text{dd}}[\Psi]$. This is by no means a simple task due to the complicated mathematical form of the dipolar interaction potential. We shall consider this in detail in the following two sections.

3.2 The dipolar interaction energy contribution in quasi-2D

In Chapter 2, we were able to evaluate the single-particle and contact interaction energy contributions in quasi-2D by substituting the quasi-2D condensate wavefunction and performing the integrals over z . This yielded an expression for the condensate energy which was dependent only on the two-dimensional condensate wavefunction $\Phi(\boldsymbol{\rho})$ — any reference to the z -coordinate was eliminated. If we attempt to follow the same process for the dipolar interaction energy contribution, we quickly encounter a problem. The integrals over z_1 and z_2 are not tractable, which means that it is not possible to eliminate references to the z -coordinates analytically. As a result, it appears as if there is no way to continue with the analysis analytically. However we need not give up yet. One alternative, which we shall now consider, is to work in reciprocal space rather than real space.

We may rewrite the dipolar interaction energy contribution in reciprocal space by applying the Fourier convolution theorem to the definition given in Equation (3.3). Thus we find that

$$E_{\text{dd}}[\Psi] = \frac{1}{2} \frac{1}{(2\pi)^3} \int d\mathbf{k} \tilde{\varrho}(\mathbf{k}) \tilde{\varrho}(-\mathbf{k}) \tilde{U}_{\text{dd}}(\mathbf{k}), \quad (3.5)$$

where \mathbf{k} is a vector in reciprocal space and an overset tilde denotes the Fourier transform: $\tilde{f}(\mathbf{k}) \equiv \int d\mathbf{r} f(\mathbf{r}) e^{-i\mathbf{k}\cdot\mathbf{r}}$ (see reference [37]). This expression for $E_{\text{dd}}[\Psi]$ already appears to be a simplification, since the double integral over real space has been reduced to a single integral over reciprocal space.

In order to evaluate Equation (3.5) in quasi-2D, we substitute the Fourier transform of the quasi-2D condensate density: $\tilde{\varrho}(\mathbf{k}) = e^{-k_z^2 l_z^2/4} \tilde{n}(\mathbf{k}_\perp)$. This expression for $\tilde{\varrho}(\mathbf{k})$ follows from the definition of the quasi-2D condensate wavefunction given in Equation (2.4). Hence we find that

$$E_{\text{dd}}[\Phi] = \frac{1}{2} \frac{1}{(2\pi)^2} \int d\mathbf{k}_\perp \tilde{n}(\mathbf{k}_\perp) \tilde{n}(-\mathbf{k}_\perp) \tilde{U}_{\text{dd}}^{2\text{D}}(\mathbf{k}_\perp), \quad (3.6)$$

where

$$\tilde{U}_{\text{dd}}^{2\text{D}}(\mathbf{k}_\perp) \equiv \frac{1}{2\pi} \int_{-\infty}^{\infty} dk_z e^{-k_z^2 l_z^2/2} \tilde{U}_{\text{dd}}(\mathbf{k}). \quad (3.7)$$

Here we note that $\mathbf{k}_\perp = k_x \hat{\mathbf{x}} + k_y \hat{\mathbf{y}}$ is the projection of \mathbf{k} onto the xy -plane — it is the reciprocal space analogue of $\boldsymbol{\rho}$.

The function $\tilde{U}_{\text{dd}}^{2\text{D}}(\mathbf{k}_\perp)$ defined above may be thought of as an effective dipolar interaction potential in two-dimensional reciprocal space. It contains the integral over k_z , which we would like to evaluate so that we may remove any lingering references to the third spatial dimension. It is in fact possible to perform this integral using special functions. Substituting the Fourier transform of the dipolar interaction potential $\tilde{U}_{\text{dd}}(\mathbf{k}) = C_{\text{dd}} \left(\hat{k}_z^2 - 1/3 \right)$, we find that

$$\tilde{U}_{\text{dd}}^{2\text{D}}(\mathbf{k}_\perp) = \frac{C_{\text{dd}}}{3\sqrt{2\pi}l_z} \left(2 - \frac{3\sqrt{2\pi}}{2} k_\perp l_z e^{\frac{k_\perp^2 l_z^2}{2}} \text{erfc} \left(\frac{k_\perp l_z}{\sqrt{2}} \right) \right), \quad (3.8)$$

where $\text{erfc}(\cdot)$ is the complementary error function.

3.3 Evaluation of the dipolar interaction energy contribution in the vortex lattice ground state

Now that we have derived an expression for the dipolar interaction energy in quasi-2D, we may evaluate the energy assuming that the condensate is in the vortex lattice ground state. Performing the Fourier transform on the vortex lattice condensate density specified in Equation (2.13), we have that

$$\tilde{n}(\mathbf{k}_\perp) = N \sum_{\mathbf{q}} \bar{g}_{\mathbf{q}} e^{-\frac{\sigma^2}{4} |\mathbf{q} - \mathbf{k}_\perp|^2}. \quad (3.9)$$

This enters into the expression for the dipolar interaction energy as a product $\tilde{n}(\mathbf{k}_\perp)\tilde{n}(-\mathbf{k}_\perp)$, which may be written as:

$$N^2 \sum_{\mathbf{q}, \mathbf{v}} \bar{g}_{\mathbf{q}} \bar{g}_{\mathbf{v}} \exp \left(-\frac{\sigma^2}{4} (\mathbf{q}^2 + \mathbf{v}^2 + 2(\mathbf{q} - \mathbf{v}) \cdot \mathbf{k}_\perp + 2\mathbf{k}_\perp^2) \right).$$

Putting this into Equation (3.6) and bringing the sums over the reciprocal lattice vectors outside the integral, we find that

$$E_{\text{dd}}(\tau, \eta) = \frac{N^2 C_{\text{dd}}}{3(2\pi)^{\frac{3}{2}} l_z^3} \sum_{\mathbf{q}, \mathbf{v}} \bar{g}_{\mathbf{q}} \bar{g}_{\mathbf{v}} e^{-\frac{\sigma^2}{4}(\mathbf{q}^2 + \mathbf{v}^2)} A(\mathbf{v} - \mathbf{q}), \quad (3.10)$$

where

$$A(\mathbf{q}) \equiv \frac{1}{2\pi} \int d\mathbf{u} e^{-\frac{\sigma^2}{i^{\frac{1}{2}}}(u^2 + \frac{1}{\sqrt{2}} l_z \mathbf{q} \cdot \mathbf{u})} [2 - 3\sqrt{\pi} u e^u \text{erfc}(u)]. \quad (3.11)$$

The integral defining $A(\mathbf{q})$ is effectively an integral over \mathbf{k}_\perp , however it has been re-expressed here in terms of the dimensionless vector $\mathbf{u} \equiv \mathbf{k}_\perp l_z / \sqrt{2}$. Writing out the integral explicitly in polar coordinates $u \equiv (u_x + u_y)^{\frac{1}{2}}$ and $\phi_u \equiv \text{atan2}(u_y, u_x)$, we have:

$$\begin{aligned} A(\mathbf{q}) &= \frac{1}{2\pi} \int_0^\infty du e^{-\frac{\sigma^2}{i^{\frac{1}{2}}} u^2} [2u - 3\sqrt{\pi} u^2 e^u \text{erfc}(u)] \int_0^{2\pi} d\phi_u e^{\frac{\sigma^2 \mathbf{q}}{\sqrt{2} l_z} u \cos \phi_u} \\ &= \int_0^\infty du e^{-\frac{\sigma^2}{i^{\frac{1}{2}}} u^2} [2u - 3\sqrt{\pi} u^2 e^u \text{erfc}(u)] I_0 \left(\frac{\sigma^2 q y}{\sqrt{2} l_z} \right) \end{aligned}$$

where $I_n(\cdot)$ is the modified Bessel function of the first kind. At this point, the integral may be separated into two terms $A_1(\mathbf{q}) + A_2(\mathbf{q})$, by expanding the factor in the square brackets. The first term has a simple solution:

$$\begin{aligned} A_1(\mathbf{q}) &\equiv 2 \int_0^\infty du u e^{-\frac{\sigma^2}{i^{\frac{1}{2}}} u^2} I_0 \left(\frac{\sigma^2 q u}{\sqrt{2} l_z} \right) \\ &= \left(\frac{l_z}{\sigma} \right)^2 e^{\frac{\sigma^2 \mathbf{q}^2}{8}}. \end{aligned} \quad (3.12)$$

However the second term given by

$$A_2(\mathbf{q}) = 3\sqrt{\pi} \int_0^\infty du u^2 e^{-\left(\frac{\sigma^2}{i^{\frac{1}{2}}} - 1\right) u^2} \text{erfc}(u) I_0 \left(\frac{\sigma^2 q u}{\sqrt{2} l_z} \right) \quad (3.13)$$

does not appear to be tractable. Whilst this does present a significant problem, we shall not concern ourselves with it at the moment. For now, we shall consider $A_2(\mathbf{q})$ to be an abstract function.

Returning to the expression for the dipolar interaction energy given in Equation (3.10), we may now substitute our simplified result for $A_1(\mathbf{q})$ to find that

$$E_{\text{dd}}(\tau, \eta) = \frac{2N^2 C_{\text{dd}}}{3(2\pi)^{\frac{3}{2}} l_z \sigma^2} \mathcal{I}(\tau, \eta) + \frac{N^2 C_{\text{dd}}}{3(2\pi)^{\frac{3}{2}} l_z^3} \mathcal{W}(\tau, \eta), \quad (3.14)$$

where $\mathcal{I}(\tau, \eta)$ is as defined in Equation (2.16) and

$$\mathcal{W}(\tau, \eta) \equiv \sum_{\mathbf{q}, \mathbf{v}} \bar{g}_{\mathbf{q}} \bar{g}_{\mathbf{v}} e^{-\frac{\sigma^2}{4}(\mathbf{q}^2 + \mathbf{v}^2)} A_2(\mathbf{v} - \mathbf{q}). \quad (3.15)$$

This is an important result because the energy has been separated into two distinct contributions: a *local contribution* which is proportional to $\mathcal{I}(\tau, \eta)$ and a *non-local contribution* which is proportional to $\mathcal{W}(\tau, \eta)$. The local contribution is so-named because it may be attributed to the *local* s-wave part of the dipolar interaction potential. We are able to make this deduction because the contribution is of the same form as the contact interaction energy contribution, albeit with a different pre-factor. Continuing this line of reasoning, the non-local contribution must then be related to the remaining non-s-wave part of the dipolar interaction potential — the *non-local* part of the interaction.

In principle, we now have everything we need to calculate the dipolar interaction energy as a function of the lattice parameters. We already know how to deal with the local contribution since it involves $\mathcal{I}(\tau, \eta)$, which we saw in Chapter 2. However the analogous function for the non-local contribution, $\mathcal{W}(\tau, \eta)$, is new to us and will turn out to present a number of difficulties. The main difficulty we shall encounter is to do with the integral that defines $A_2(\mathbf{q})$, which we flagged as being problematic earlier on. Since this integral is not tractable, it must be evaluated numerically. This in itself is not an issue, however unfortunately the integral has poor convergence properties, which means that it takes an unreasonable amount of time to obtain an accurate solution. In order to get around problems such as this one, we must think of a cleverer way to implement $\mathcal{W}(\tau, \eta)$ numerically. This will be the subject of the following section.

3.4 Solution to numerical issues

There are three issues regarding the numerical evaluation of $\mathcal{W}(\tau, \eta)$ which we would like to overcome. They are:

1. *Poor convergence of the integral specifying $A_2(\mathbf{v} - \mathbf{q})$.*

It takes of order seconds to obtain a convergent solution to the integral using the `NIntegrate` function in *Mathematica*. This is an excessive amount of time because we must evaluate the same integral for many values of $\mathbf{v} - \mathbf{q}$.

2. *Prevalence of extremely large and extremely small numbers.*

For the parameter ranges we shall consider, $A_2(\mathbf{v} - \mathbf{q})$ can be as large as $10^{+600000}$ whilst the factor $e^{-\frac{\sigma^2}{4}(\mathbf{v}^2 + \mathbf{q}^2)}$ is as small as $10^{-600000}$. It would be beneficial if we could avoid

working with such large numbers, because the product $e^{-\frac{\sigma^2}{4}(\mathbf{v}^2+\mathbf{q}^2)}A_2(\mathbf{v}-\mathbf{q})$ (which we ultimately need to calculate) is in fact a reasonably-sized number.

3. *An overabundance of terms in the sum over \mathbf{q} and \mathbf{v} .*

The double sum over the reciprocal lattice vectors requires calculating an unwieldy number of terms. Ideally, we would like to make a similar approximation to the one we made in the calculation of $\mathcal{I}(\tau, \eta)$ where the double sum was collapsed by setting $\mathbf{q} = -\mathbf{v}$.

Addressing each of these issues in detail is rather tedious and not particularly illuminating, so we shall only discuss some of the key points here.

In order to resolve the first issue, we essentially break up the difficult integral into a series of simpler integrals, each of which is analytically solvable. This is done by expressing the complementary error function, which appears in the integrand, as a power series:

$$\operatorname{erfc}(u) = 1 - \frac{2}{\sqrt{\pi}} \sum_{n=0}^{\infty} \frac{(-1)^n u^{2n+1}}{n!(2n+1)}. \quad (3.16)$$

We then bring the sum over n outside the integral and do the resultant integral to yield an expression for $A_2(\mathbf{v}-\mathbf{q})$ of the form: $\sum_{n=0}^{\infty} a_n(\mathbf{v}-\mathbf{q})$. Of course, this series is not necessarily guaranteed to converge, because it is not always appropriate to reverse the order of summation and integration. Fortunately there are no issues with convergence in this case. In fact we find that the series itself has excellent convergence properties: it may be truncated at small n whilst still maintaining a high level of accuracy, which should make fast evaluation possible.

Addressing the second issue, regarding extremely large and extremely small numbers, is relatively simple. Rather than working with $A_2(\mathbf{v}-\mathbf{q})$ and $e^{-\frac{\sigma^2}{4}(\mathbf{v}^2+\mathbf{q}^2)}$ individually, we consider the product $e^{-\frac{\sigma^2}{4}(\mathbf{v}^2+\mathbf{q}^2)}A_2(\mathbf{v}-\mathbf{q})$ analytically as a single object. Using the power series expression for $A_2(\mathbf{v}-\mathbf{q})$, it is possible to cancel out $e^{-\frac{\sigma^2}{4}(\mathbf{v}^2+\mathbf{q}^2)}$ with other factors in the terms of the series. One then obtains a new power series for the product $e^{-\frac{\sigma^2}{4}(\mathbf{v}^2+\mathbf{q}^2)}A_2(\mathbf{v}-\mathbf{q})$, where each term in the series may be evaluated at machine precision.

The final issue is resolved by collapsing the double sum over \mathbf{q} and \mathbf{v} , assuming that $\mathbf{q} = -\mathbf{v}$. This approximation is valid in the limit $\sigma^2\mathbf{q}^2 \gg 1$, which is true in the limit of large vortex number. In order to prove that this is a reasonable approximation to make, one can evaluate $e^{-\frac{\sigma^2}{4}(\mathbf{v}^2+\mathbf{q}^2)}A_2(\mathbf{v}-\mathbf{q})$ as indicated above, and observe that the resulting expression is greatest in magnitude when $\mathbf{q} = -\mathbf{v}$. The terms in the sum for which $e^{-\frac{\sigma^2}{4}(\mathbf{v}^2+\mathbf{q}^2)}A_2(\mathbf{v}-\mathbf{q})$ is greatest in magnitude are the most dominant contributions, however the smaller terms for which $\mathbf{q} \neq -\mathbf{v}$ may reasonably be neglected.

Combining these resolutions, we find that

$$\mathcal{W}(\tau, \eta) \approx \sum_{\mathbf{q}} (\bar{g}_{\mathbf{q}})^2 \left(e^{-\frac{\sigma^2\mathbf{q}^2}{2}} A_2^a(2\mathbf{q}) + e^{-\frac{\sigma^2\mathbf{q}^2}{2}} A_2^b(2\mathbf{q}) \right) \quad (3.17)$$

where

$$e^{-\frac{\sigma^2 \mathbf{q}^2}{2}} A_2^a(2\mathbf{q}) = \frac{3\pi}{8(\beta^2 - 1)^{\frac{5}{2}}} e^{-\frac{(\beta^2 - 2)\mathbf{q}^2 \sigma^2}{4(\beta^2 - 1)}} \\ \times \left[\beta^4 l_z^2 \mathbf{q}^2 I_1 \left(\frac{\beta^4 l_z^2 \mathbf{q}^2}{4 - 4\beta^2} \right) - (2\beta^2 + \beta^4 l_z^2 \mathbf{q}^2 - 2) I_0 \left(\frac{\beta^4 l_z^2 \mathbf{q}^2}{4 - 4\beta^2} \right) \right]$$

and

$$e^{-\frac{\sigma^2 \mathbf{q}^2}{2}} A_2^b(2\mathbf{q}) = 3 e^{-\frac{\mathbf{q}^2 \sigma^2}{2(\beta^2 - 1)}} \sum_{n=0}^{\infty} \frac{(-1)^n (n+1)}{(\beta^2 - 1)^{2+n} (2n+1)} L_{1+n} \left(\frac{\beta^4 l_z^2 \mathbf{q}^2}{2 - 2\beta^2} \right).$$

Here, $\beta \equiv \sigma/l_z$ and $L_n(\cdot)$ is the n -th Laguerre polynomial. This series expression for $\mathcal{W}(\tau, \eta)$ is about 300 times faster to evaluate than if we were to numerically integrate $A_2(2\mathbf{q})$.

3.5 Optimal vortex lattice geometry

3.5.1 Preliminary setup

With the results of the previous section, we now have a computationally efficient implementation of the condensate energy in the vortex lattice ground state. This means that it is now feasible, from a computational perspective, to numerically minimise the condensate energy, $E(\tau, \eta) = E_0 + E_{\text{int}}(\tau, \eta)$, with respect to τ and η to determine the optimal vortex lattice geometry. In minimising the condensate energy we need only consider the interaction energy contribution, $E_{\text{int}}(\tau, \eta)$, since the single-particle contribution, E_0 , does not depend on τ and η .

Adding together the expressions for $E_{\text{cont}}(\tau, \eta)$ and $E_{\text{dd}}(\tau, \eta)$, given in Equations (2.15) and (3.14) respectively, we have that the interaction energy contribution is given by:

$$E_{\text{int}}(\tau, \eta) = \frac{N^2 C_{\text{dd}}}{3(2\pi)^{\frac{3}{2}} l_z^3} \left[\left(2 + \frac{1}{\epsilon_{\text{dd}}} \right) \left(\frac{l_z}{\sigma} \right)^2 \mathcal{I}(\tau, \eta) + \mathcal{W}(\tau, \eta) \right]. \quad (3.18)$$

Here we have introduced the parameter $\epsilon_{\text{dd}} \equiv C_{\text{dd}}/3g$ which quantifies the relative strength of the dipolar and contact interactions. In the work that follows, we shall assume $C_{\text{dd}} > 0$ so that the factor outside the square brackets is also positive. This allows us to define a dimensionless analogue of the interaction energy contribution:

$$\bar{E}_{\text{int}}(\tau, \eta) \equiv \left(2 + \frac{1}{\epsilon_{\text{dd}}} \right) \left(\frac{l_z}{\sigma} \right)^2 \mathcal{I}(\tau, \eta) + \mathcal{W}(\tau, \eta), \quad (3.19)$$

which may be minimised in place of $E_{\text{int}}(\tau, \eta)$. We note that the case where $C_{\text{dd}} < 0$ requires more careful treatment, since the sign of $\bar{E}_{\text{int}}(\tau, \eta)$ becomes opposite to the sign of $E_{\text{int}}(\tau, \eta)$, meaning that the maxima and minima are inverted.

	$v_c/\pi l_\rho^2$	l_ρ/l_z	σ/l_z
(a)	1.01908	40	292.331...
(b)	1.01908	80	584.662...

Table 3.1: Relationships between the length scales l_ρ , l_z and σ , for the two cases (a) and (b) which we shall consider in the minimisation of the condensate energy. Note that $v_c = \pi\sigma^2/(l_\rho\sigma^2 - 1)$.

The notation that we have adopted for $\bar{E}_{\text{int}}(\tau, \eta)$ makes it clear that there is a dependence on τ and η . However it conceals the fact that there is also a dependence on four additional parameters: ϵ_{dd} , l_ρ , l_z and σ . Whilst it is likely that the optimal vortex lattice geometry depends on each of these four additional parameters in some way, it is only practical from a computational perspective to allow one to vary at a time. Since there are strict conditions on the length scales in the problem, we shall opt to fix l_ρ , l_z and σ , whilst allowing ϵ_{dd} to vary.

In fixing the length scales, we must satisfy two criteria which are related to our previous assumptions:

- (i) $v_c/\pi l_\rho^2 \rightarrow 1^+$: this ensures that the condensate is in the fast-rotating limit, where a large number of vortices are present.
- (ii) $l_\rho/l_z \gg 1$: this corresponds to a highly oblate trap, and ensures that the condensate is in the quasi-2D limit.

In order to satisfy the first criterion, we shall arbitrarily set $v_c/\pi l_\rho^2 = 1.01908$ throughout our analysis. For the second criterion we shall consider two possibilities: (a) $l_\rho/l_z = 40$ and (b) $l_\rho/l_z = 80$. By fixing l_ρ in addition to criteria (i) and (ii), we may fully specify all of the length scales in the problem. A summary of the relationships between the length scales is given in Table 3.1 for the two cases we shall consider.

3.5.2 Results and discussion

We perform the numerical minimisation over a range of values of ϵ_{dd} for both sets of length scales specified in Table 3.1. The results are shown in Figures 3.1(a) and (b), for the length scales in rows (a) and (b) of the table, respectively. In both figures, the optimal values of τ and η are plotted against $1/\epsilon_{\text{dd}}$ ¹. The optimal value of τ is represented by a *solid* line with reference to the scale on the *left* vertical axis, while the optimal value of η is represented by a *dotted* line with reference to the scale on the *right* vertical axis. Taken together, the optimal values of τ and η describe the optimal vortex lattice geometry.

By comparing the optimal values of τ and η to the standard lattice parametrisations given in Figure 2.3, we are able to classify the geometry of the vortex lattice. For example, at the point $1/\epsilon_{\text{dd}} = -1.82$ in Figure 3.1(a), we find that a square lattice is favourable since the optimal values of τ and η at that point are 1 and $\frac{\pi}{2}$ respectively. Continuing in this way, we

¹We plot the optimal lattice parameters against $1/\epsilon_{\text{dd}}$ rather than ϵ_{dd} itself to avoid a divergence at $\epsilon_{\text{dd}} = 0$.

see that three types of lattice may occur depending on the value of $1/\epsilon_{\text{dd}}$: triangular, square or rectangular.² Each of these lattice geometries occurs in a distinct region of the phase space, which we indicate by coloured shading in the figure. Comparing Figures 3.1(a) and (b), we see that the relative size of each region is the same for both sets of length scales. There is however an overall translation and scaling difference between the two cases: the regions in Figure 3.1(b) are contracted and shifted to the left compared to those in Figure 3.1(a). A more accurate description of the phase regions is given in Table 3.2 in terms of inequalities.

In addition to the three colour-shaded regions, there is also a grey-shaded region for which the condensate is in the so-called *collapse phase*. In the collapse phase, the optimal value of τ tends to zero and our vortex lattice analysis begins to break down. Physically, this phase corresponds to a situation where the vortices are arranged in densely-packed lines, with the spacing between the lines being larger than the extent of the condensate in the xy -plane. Since the unit cell of the lattice extends beyond the boundaries of the condensate in this situation, we say that the vortex lattice has “collapsed”.

When the system enters the collapse phase, there are also signs from a computational perspective that our analysis becomes invalid. Since τ approaches zero in this phase, our expression for $\bar{E}_{\text{int}}(\tau, \eta)$ becomes inaccurate because we only included enough terms in the Fourier decomposition to consider values of τ greater than about 0.05 (we cut off the sums at $M = 15$). Incidentally, this is why we do not see τ approaching zero in the grey collapse region in Figures 3.1(a) and (b) — because we constrained the minimisation to values of τ greater than 0.05, where our expression for $\bar{E}_{\text{int}}(\tau, \eta)$ is reliable. In order to approach $\tau = 0$, we would need to include a near-infinite number of terms ($M \gg 15$) in our expression for $\bar{E}_{\text{int}}(\tau, \eta)$, which is computationally impractical. This poor convergence is indicative of a problem with the theory at the point $\tau = 0$.

Apart from the stability of the vortex lattice, we may also assess the stability of the condensate itself by looking at the sign of $E_{\text{int}}(\tau, \eta)$. If $E_{\text{int}}(\tau, \eta)$ is negative, then we shall regard the condensate as being prone to collapse. This is only an approximate way of assessing stability, but it will be good enough for our purposes³. The region of phase space for which $E_{\text{int}}(\tau, \eta)$ is negative is the area to the left of the red line in Figures 3.1(a) and (b). Interestingly, we see that $E_{\text{int}}(\tau, \eta)$ becomes negative at roughly the value of $1/\epsilon_{\text{dd}}$ where the optimal value of τ approaches zero. This suggests that there is a strong link between the collapse of the condensate and the collapse of the vortex lattice.

3.6 Summary

We have analysed vortex lattice geometry in dipolar BECs for the special case of on-axis polarisation. The results show that three lattice geometries are possible, depending on the

²A visualisation of the condensate density for each of these lattice geometries is shown on the cover of this thesis (top left circle: triangular, top right circle: square, bottom left circle: rectangular).

³Ideally we should consider the sign of the total energy $E(\tau, \eta) = E_0 + E_{\text{int}}(\tau, \eta)$, however this would require us to calculate E_0 , which depends on system-specific parameters such as the mass and total number of particles (see Equation (2.14)).

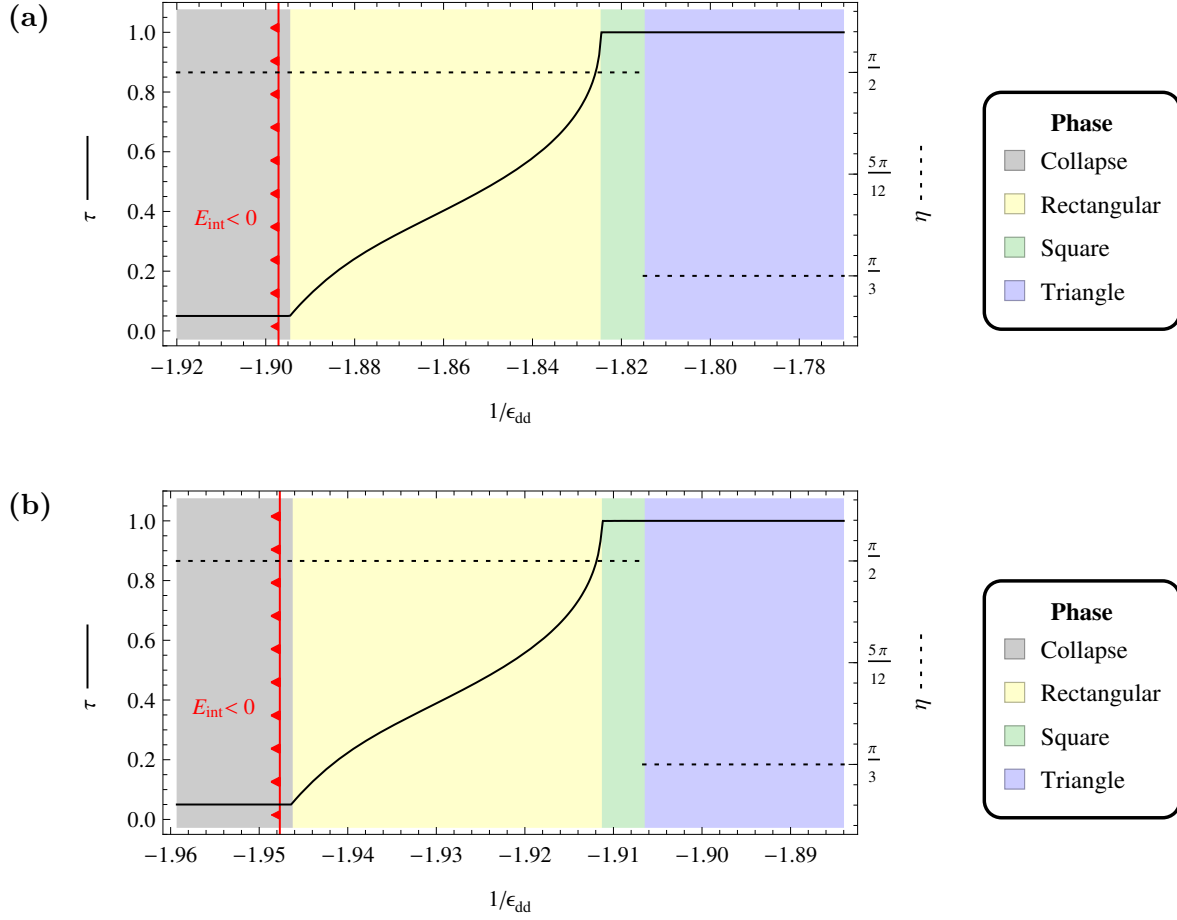


Figure 3.1: Plots showing the optimal values of τ and η in dipolar BECs with on-axis polarisation. Plot (a) assumes the length scales in row (a) of Table 3.1 and plot (b) assumes the length scales in row (b). In each plot, the black solid (dashed) line represents the optimal value of τ (η) with reference to the scale on the left (right) vertical axis. By classifying the (τ, η) parameters, four distinct regions in phase space are identified: a collapse phase, rectangular lattice (stripe) phase, square lattice phase, and triangular lattice phase. These regions are indicated by coloured shading. The red line with arrows on the left side specifies the region for which $E_{\text{int}}(\tau, \eta) < 0$.

Phase	Parameter range	
	Figure 3.1(a)	Figure 3.1(b)
Collapse	$1/\epsilon_{\text{dd}} < -1.8945$	$1/\epsilon_{\text{dd}} < -1.9462$
Rectangular	$-1.8945 < 1/\epsilon_{\text{dd}} < -1.8247$	$-1.9462 < 1/\epsilon_{\text{dd}} < -1.9113$
Square	$-1.8247 < 1/\epsilon_{\text{dd}} < -1.8149$	$-1.9113 < 1/\epsilon_{\text{dd}} < -1.9065$
Triangular	$1/\epsilon_{\text{dd}} > -1.8149$	$1/\epsilon_{\text{dd}} > -1.9065$

Table 3.2: Definition of the four regions in phase space shown in Figures 3.1(a) and (b) in terms of inequalities.

value of $1/\epsilon_{\text{dd}}$ and the values of the length scales l_ρ , l_z and σ . In general, we find that a triangular lattice geometry is favoured in regions where the local interaction contribution dominates, as was seen in the non-dipolar case. However, in regions where the non-local interaction contribution becomes significant, the favoured lattice geometries changes from triangular to square or rectangular. Below a certain value of $1/\epsilon_{\text{dd}}$ (corresponding to reasonably strong, attractive contact interactions) the vortex lattice and the condensate appear to collapse concurrently, although our analysis is not reliable in this region.

The results that we have obtained appear to qualitatively agree with previous results of Zhang and Zhai [1] and Cooper et al. [2]. Zhang and Zhai also find that the lattice geometry undergoes a transition from triangular \rightarrow square \rightarrow rectangular \rightarrow collapse as the value of $1/\epsilon_{\text{dd}}$ decreases. It is difficult, however, to make a quantitative comparison between our results because Zhang and Zhai do not mention the values of the length scales that they used. Cooper et al. also find the same transitions between lattice geometries. However, they do not find that the lattice collapses after passing through the rectangular lattice phase. Instead, they observe a bubble phase — a different kind of periodic vortex structure in which the vortices are arranged around “bubbles” of high particle density. It is not surprising that we do not see the bubble phase in our results, because it is not a vortex lattice phase: it falls outside the scope of our analytic treatment.

Yi and Pu also conducted a similar study of vortex lattice geometry based on numerical simulations of the GP equation, however their results are not in agreement with those obtained here, nor with those of Zhang and Zhai and Cooper et al. They only observe triangular lattice geometries in their simulations, and conclude that the square and rectangular lattice geometries do not exist. A possible explanation for this discrepancy, is that the particular parameter values they chose for their simulations did not fall in the square and rectangular lattice regions. It is very difficult based on numerical simulations alone to investigate the entire parameter space thoroughly.

The surest way to resolve this discrepancy is by performing experiments, however it does not appear as if any experimental groups are currently working towards producing fast-rotating dipolar BECs. In the absence of experimental proof, it would be worthwhile to conduct further numerical simulations based on insight from our analytic results.

Chapter 4

Vortex lattices in dipolar BECs with off-axis polarisation

In this chapter, we shall extend our analysis of vortex lattices in dipolar BECs to consider the more general case of *off-axis polarisation*. In this case, the dipole polarisation vector, $\hat{\mathbf{p}}$, is no longer fixed along the axis of rotation, but is permitted to point in any direction in the rotating frame. By allowing $\hat{\mathbf{p}}$ to vary in this way, we are able to explore a much larger range of the parameter space of dipolar BECs. In fact, if we simultaneously allow ϵ_{dd} to vary, then we are able to almost completely cover the entire parameter space, within the bounds of our initial assumptions¹.

4.1 Parametrisation of the dipole polarisation

In order to begin to consider the case of off-axis polarisation, we must first choose an appropriate parametrisation for the dipole polarisation vector, $\hat{\mathbf{p}}$. Since $\hat{\mathbf{p}}$ is a three-dimensional unit vector, it would ordinarily be described in terms of two parameters; for example an azimuthal and polar angle. However due to the cylindrical symmetry of the condensate, it is convenient to fix the azimuthal angle, so that $\hat{\mathbf{p}}$ is described solely in terms of the polar angle. Here we shall choose to fix the azimuthal angle so that the y -component of $\hat{\mathbf{p}}$ vanishes. We then have that $\hat{\mathbf{p}} = \cos \alpha \hat{\mathbf{z}} + \sin \alpha \hat{\mathbf{x}}$, where α denotes the polar angle as measured from the positive z -axis. It is also important to realise that $\hat{\mathbf{p}}$ rotates along with the condensate so that it is stationary only in the rotating reference frame.

With this parametrisation for $\hat{\mathbf{p}}$, the dipolar interaction potential given in Equation (1.5) becomes:

$$U_{\text{dd}}(\mathbf{r}) = \frac{C_{\text{dd}}}{4\pi} \frac{1 - 3(\cos \alpha \cos \theta + \sin \alpha \sin \theta \cos \phi)^2}{r^3} \quad (4.1)$$

¹See Section 1.6. In addition to these assumptions, we shall not explore the region of parameter space for which C_{dd} is negative.

where the vector \mathbf{r} is expressed in spherical coordinates (r, θ, ϕ) . This expression for $U_{\text{dd}}(\mathbf{r})$ is significantly more complicated than the one we saw in the previous chapter for the case of on-axis polarisation. Nevertheless, it is possible to proceed with the analysis by following the same procedure used in the previous chapter.

4.2 Re-evaluating the dipolar interaction energy contribution in the vortex lattice ground state

In order to account for the more general form of the dipolar interaction potential given in Equation (4.1), we must re-evaluate the dipolar interaction energy contribution from scratch. The quasi-2D expression derived in the previous chapter,

$$E_{\text{dd}}[\Phi] = \frac{1}{2} \frac{1}{(2\pi)^2} \int d\mathbf{k}_{\perp} \tilde{n}(\mathbf{k}_{\perp}) \tilde{n}(-\mathbf{k}_{\perp}) \tilde{U}_{\text{dd}}^{2\text{D}}(\mathbf{k}_{\perp}) \quad (4.2)$$

remains valid, however we must re-calculate $\tilde{U}_{\text{dd}}^{2\text{D}}(\mathbf{k}_{\perp})$ for the new dipolar interaction potential according to the definition given in Equation (3.7). After some work, it is possible to show that

$$\tilde{U}_{\text{dd}}^{2\text{D}}(\mathbf{k}_{\perp}) = \frac{C_{\text{dd}}}{3\sqrt{2\pi}l_z} \left[\cos^2(\alpha) F_{\parallel} \left(\frac{\mathbf{k}_{\perp} l_z}{\sqrt{2}} \right) + \sin^2(\alpha) F_{\perp} \left(\frac{\mathbf{k}_{\perp} l_z}{\sqrt{2}} \right) \right], \quad (4.3)$$

where we have defined an on-axis contribution $F_{\parallel}(\mathbf{u}) = 2 - 3\sqrt{\pi}ue^{u^2} \text{erfc}(u)$ and an off-axis contribution $F_{\perp}(\mathbf{u}) = -1 + 3\sqrt{\pi}u_x^2 e^{u^2} \text{erfc}(u)/u$.

The next step in the analysis is to substitute the Fourier transform of the vortex lattice condensate density, given in Equation (3.9), into our new expression for $E_{\text{dd}}[\Phi]$. After simplifying the resulting expression, we eventually find that

$$E_{\text{dd}}(\tau, \eta) = \frac{N^2 C_{\text{dd}}}{3(2\pi)^{\frac{3}{2}} l_z^3} \left[\left(\frac{1 + 3 \cos(2\alpha)}{2} \right) \left(\frac{l_z}{\sigma} \right)^2 \mathcal{I}(\tau, \eta) + \mathcal{W}(\tau, \eta) \right], \quad (4.4)$$

where $\mathcal{I}(\tau, \eta)$ and $\mathcal{W}(\tau, \eta)$ are as defined previously in Equations (2.16) and (3.15). There is however a slight difference in the form of $\mathcal{W}(\tau, \eta)$, in that the function $A_2(\mathbf{q})$ which appears in the definition must be replaced by:

$$A_2(\mathbf{q}) = \frac{3}{2\sqrt{\pi}} \int_0^{\infty} du \int_0^{2\pi} d\phi_u \left\{ u^2 \text{erfc}(u) [\sin^2(\alpha) \cos^2(\phi_u) - \cos^2(\alpha)] \right. \\ \left. \times \exp \left[- \left(\frac{\sigma^2}{l_z^2} - 1 \right) u^2 - \frac{\sigma^2 q u}{\sqrt{2} l_z} \cos(\phi_u - \phi_q) \right] \right\}, \quad (4.5)$$

where we have expressed the vector \mathbf{q} in polar coordinates: (q, ϕ_q) .

As was the case in the previous chapter, the integral defining $A_2(\mathbf{q})$ is not tractable and converges poorly when evaluated numerically. In order to evaluate $\mathcal{W}(\tau, \eta)$ efficiently, we must therefore make a number of approximations similar to those outlined in Section 3.4.

Omitting the mathematical details, we eventually find that

$$\mathcal{W}(\tau, \eta) \approx \sum_{\mathbf{q}} (\bar{g}_{\mathbf{q}})^2 \left(e^{-\frac{\sigma^2 \mathbf{q}^2}{2}} A_2^a(2\mathbf{q}) + e^{-\frac{\sigma^2 \mathbf{q}^2}{2}} A_2^b(2\mathbf{q}) \right), \quad (4.6)$$

where

$$\begin{aligned} e^{-\frac{\sigma^2 \mathbf{q}^2}{2}} A_2^a(2\mathbf{q}) &= \frac{3\pi}{32(\beta^2 - 1)^{\frac{5}{2}}} e^{-\frac{(\beta^2 - 2)\mathbf{q}^2 \sigma^2}{4(\beta^2 - 1)}} \\ &\times \left\{ I_1 \left(\frac{l_z^2 \mathbf{q}^2 \beta^4}{4 - 4\beta^2} \right) [\beta^4 l_z^2 \mathbf{q}^2 (3 \cos(2\alpha) + 1) - 2 \sin^2(\alpha) \cos(2\phi_q) (2 - 2\beta^2 + \beta^4 l_z^2 \mathbf{q}^2)] \right. \\ &\quad \left. - I_0 \left(\frac{l_z^2 \mathbf{q}^2 \beta^4}{4 - 4\beta^2} \right) [(3 \cos(2\alpha) + 1)(2\beta^2 + \beta^4 l_z^2 \mathbf{q}^2 - 2) - 2\beta^4 l_z^2 \mathbf{q}^2 \sin^2(\alpha) \cos(2\phi_q)] \right\} \end{aligned}$$

and

$$\begin{aligned} e^{-\frac{\sigma^2 \mathbf{q}^2}{2}} A_2^b(2\mathbf{q}) &= -\frac{3}{2} e^{-\frac{\mathbf{q}^2 \sigma^2}{2(1-\beta^2)}} \sum_{n=0}^{\infty} \frac{(-1)^n (n+1)}{(\beta^2 - 1)^{2+n} (2n+1)} \\ &\times \left\{ \sin^2(\alpha) \cos(2\phi_q) {}_1F_1 \left(-n; 2; \frac{l_z^2 \mathbf{q}^2 \beta^4}{2 - 2\beta^2} \right) \right. \\ &\quad \left. + 2 (\cos^2(\alpha) - \sin^2(\alpha) \cos^2(\phi_q)) L_{n+1} \left(\frac{\beta^4 l_z^2 \mathbf{q}^2}{2 - 2\beta^2} \right) \right\}. \end{aligned}$$

4.3 Optimal vortex lattice geometry

The determination of the optimal vortex lattice geometry proceeds in a similar manner to the on-axis polarisation case. As before, we define a dimensionless analogue of the interaction energy contribution, given by

$$\bar{E}_{\text{int}}(\tau, \eta) = \left(\frac{1 + 3 \cos(2\alpha)}{2} + \frac{1}{\epsilon_{\text{dd}}} \right) \left(\frac{l_z}{\sigma} \right)^2 \mathcal{I}(\tau, \eta) + \mathcal{W}(\tau, \eta), \quad (4.7)$$

which may be minimised in place of the total condensate energy $E(\tau, \eta) = E_0 + E_{\text{int}}(\tau, \eta)$. However, in order for this to be valid, we must continue to assume that the dipolar interaction strength, C_{dd} , is positive.

It is important to recognise, once again, that the expression for $\bar{E}_{\text{int}}(\tau, \eta)$ given above depends on a number of parameters in addition to τ and η . These parameters are the length scales, l_ρ , l_z and σ ; the relative strength of the contact to dipolar interaction, ϵ_{dd} ; and the polarisation angle α . In the subsequent analysis, we shall fix the length scales to the values given in row (a) of Table 3.1. Ultimately, we would like to allow the remaining two parameters, ϵ_{dd} and α , to vary continuously across a broad range of values. However to begin with, we shall set $\alpha = \frac{\pi}{2}$ so that we may examine the ‘‘most extreme’’ case of off-axis polarisation in detail.

4.3.1 Dipole polarisation in the plane of rotation

For the case of off-axis polarisation where $\alpha = \frac{\pi}{2}$, the dipole polarisation vector is fixed in the plane of rotation — the xy -plane in our coordinate system. In order to visualise the optimal vortex lattice geometry in this situation, we may plot the optimal values of τ and η as a function of $1/\epsilon_{\text{dd}}$, as we did for the case of on-axis polarisation ($\alpha = 0$) in Figure 3.1. In generating the plot, we shall continue to use the same representation for the optimal values of τ and η , and the various phases of the system as we did previously. The result is shown in Figure 4.1. Looking at this figure, we immediately notice a number of differences compared to the corresponding figure for the case of on-axis polarisation (Figure 3.1(a)).

Perhaps the most noticeable difference is the fact that only two lattice geometries are observable for the $\alpha = \frac{\pi}{2}$ case: the triangular and square geometries. The rectangular lattice (stripe phase) region, which appears in Figure 3.1(a), is completely absent in Figure 4.1. This does not necessarily imply that there is no rectangular lattice region for the $\alpha = \frac{\pi}{2}$ case, however if one does exist, then it must have a width smaller than the horizontal resolution of the plot ($\Delta 1/\epsilon_{\text{dd}} = 0.005$). If a rectangular lattice region truly does not exist, then this would be a rather interesting situation from a physical perspective. Without a rectangular lattice region between the collapse phase and square lattice regions, the vortex lattice undergoes a sudden collapse as the value of $1/\epsilon_{\text{dd}}$ decreases. This is evident from the fact that the phase parameter, τ , jumps discontinuously, rather than smoothly falling from 1 to approximately zero.

Another point of difference between Figures 4.1 and 3.1(a) is the width and location of the phase boundaries. In Figure 4.1, the collapse boundary, and the boundary between the square and triangular lattice regions, are both shifted in the positive $1/\epsilon_{\text{dd}}$ direction compared to those in Figure 3.1(a). This means that the phase boundaries occur at positive values of $1/\epsilon_{\text{dd}}$ for the $\alpha = \frac{\pi}{2}$ case, rather than at negative values as we saw for the case of on-axis polarisation. The particular values of $1/\epsilon_{\text{dd}}$ at which the phase boundaries occur for the $\alpha = \frac{\pi}{2}$ case are given in Table 4.1. It is interesting to note that the non-triangular lattice phases (i.e. the collapse phase and the square lattice phase) both occur for values of $1/\epsilon_{\text{dd}} < 1$. This happens to correspond to the values of $1/\epsilon_{\text{dd}}$ where the dipolar interaction dominates over the contact interaction.

As yet, we have not taken into consideration the stability of the condensate itself. According to our previous definition, the condensate is deemed to be unstable if $E_{\text{int}} < 0$ and stable otherwise. Looking at the red line in Figure 4.1, we see that the unstable region occurs for values of $1/\epsilon_{\text{dd}}$ less than about 0.97. This is very different from the case of on-axis polarisation, where the $E_{\text{int}} = 0$ line and the collapse phase boundary were found to occur at roughly the same value of $1/\epsilon_{\text{dd}}$. For the $\alpha = \frac{\pi}{2}$ case, we see that the condensate becomes unstable *before* the square lattice phase and collapse phase are able to occur. This would suggest that the square lattice phase cannot be supported by a condensate with $\alpha = \frac{\pi}{2}$.

We should be careful to note, however, that our classification of stability based on the sign of E_{int} only provides us with an *indication* of the stability of the condensate. It may be possible for the condensate to be stable even if $E_{\text{int}} < 0$, provided that E_0 is large enough so that the total energy $E = E_0 + E_{\text{int}}$ is positive. However, since E_0 is system-specific (it depends on

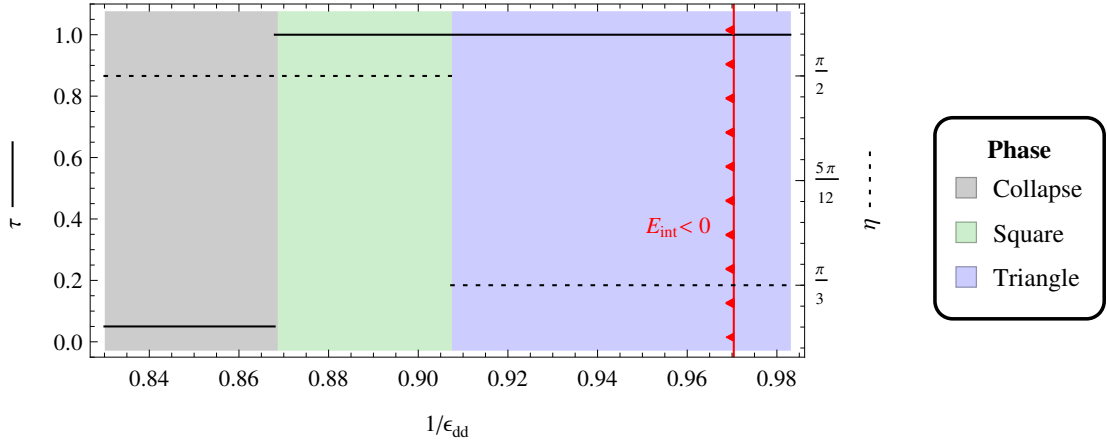


Figure 4.1: Plot showing the optimal values of τ and η in dipolar BECs with polarisation in the plane of rotation ($\alpha = \frac{\pi}{2}$). The length scales l_ρ , l_z and σ are assumed to satisfy the relations in row (a) of Table 3.1. The black solid (dashed) line represents the optimal value of τ (η) with reference to the scale on the left (right) vertical axis. The coloured shading identifies the phase which corresponds to the optimal (τ, η) values in the region. The red line with arrows on the left side specifies the region for which $E_{\text{int}}(\tau, \eta) < 0$.

Phase	Parameter range
Collapse	$1/\epsilon_{\text{dd}} < 0.8687$
Square	$0.8687 < 1/\epsilon_{\text{dd}} < 0.9075$
Triangular	$1/\epsilon_{\text{dd}} > 0.9075$

Table 4.1: Definition of the three regions in phase space shown in Figure 4.1 in terms of inequalities.

the mass and total number of particles among other variables as is shown in Equation (2.14)), it is not possible for us to give a more accurate evaluation of stability based on the total energy E , without specialising our results.

4.3.2 Varying the dipole polarisation

In this section, we shall perform the minimisation of $\bar{E}_{\text{int}}(\tau, \eta)$ whilst allowing both α and ϵ_{dd} to vary over a large range of values. In doing so, we shall construct a phase diagram for the optimal vortex lattice geometry in the $(1/\epsilon_{\text{dd}}, \alpha)$ parameter space. As mentioned previously, this will allow us to almost completely explore the parameter space of vortex lattices in dipolar BECs within the bounds of our initial assumptions.

In order to construct a phase diagram for the optimal vortex lattice geometry, we must calculate the optimal values of τ and η over a wide range of $(1/\epsilon_{\text{dd}}, \alpha)$ values. From a computational perspective, it is not at all efficient to do this on a uniform grid, because there are jump discontinuities in the optimal values of τ and η which may only be resolved at high resolution. To resolve these features clearly and efficiently, we shall use a technique called

adaptive sampling. This involves sampling more points where the optimal values of τ and η are found to vary significantly, and fewer points elsewhere.

In total, we perform the minimisation at 9835 points within the region: $-2.1 \leq 1/\epsilon_{\text{dd}} \leq 1.1$ and $0 \leq \alpha \leq \frac{\pi}{2}$. In order to calculate the phase boundaries, we apply an interpolation function to the optimal values of τ and η , and extracting the appropriate contours. For example, to calculate the collapse boundary, we extract the points for which the optimal value of τ is minutely above 0.05. We then use these points to generate a B-spline curve which yields a smooth phase boundary. Applying a similar procedure to calculate the other phase boundaries, we obtain the phase diagram shown in Figure 4.2. In this figure, we have only plotted the vortex lattice phases — we have not included the optimal values of τ and η .

Looking at the figure, we essentially see a smooth transition between the two cases we have already studied: the case of on-axis polarisation ($\alpha = 0$) and the case of polarisation in the plane of rotation ($\alpha = \frac{\pi}{2}$). At the bottom of the plot, where $\alpha = 0$, the rectangular, square and triangular lattice geometries are possible. As α increases, the rectangular lattice region becomes narrower in width, until it eventually disappears at $\alpha \approx \frac{3\pi}{16}$. Coincidentally, at approximately the same value of α , the red $E_{\text{int}} = 0$ line also begins to separate from the collapse phase boundary. It continues this trend as the value of α increases further.

4.4 Summary

We have extended our analysis of vortex lattice geometry in dipolar BECs to consider the case of off-axis dipole polarisation. The results show that the lattice geometry varies significantly as a function of the dipole polarisation angle α . Specifically, we find that the rectangular lattice region decreases in width as α increases above zero, until it eventually vanishes at $\alpha \approx \frac{3\pi}{16}$. This means that only the triangular and square lattice geometries are possible in situations where the dipole polarisation is tilted far off-axis.

In addition, we assessed the stability of the BEC based on the sign of the interaction energy contribution. This allowed us to determine whether or not the BEC could support the vortex lattice in particular regions of the phase space. From these considerations, we concluded that the BEC is prone to collapse in the square lattice region when the dipole polarisation is tilted far off-axis. This means that it is not always possible for a dipolar BEC to support a square vortex lattice geometry in the off-axis case. It is only possible if conditions are favourable, so that the single-particle energy contribution is large enough to stabilise the system.

There is only one related study by Yi and Pu [28], with which we may compare the results obtained in this chapter. Yi and Pu do not consider off-axis polarisation arbitrarily, however they do consider the special case where the polarisation is in the plane of rotation ($\alpha = \frac{\pi}{2}$). Through numerical simulation of the GP equation, they find that a square lattice geometry is favoured. This supports our findings, however we should be careful to note that Yi and Pu's simulation was not strictly in the fast-rotating limit that we have assumed.

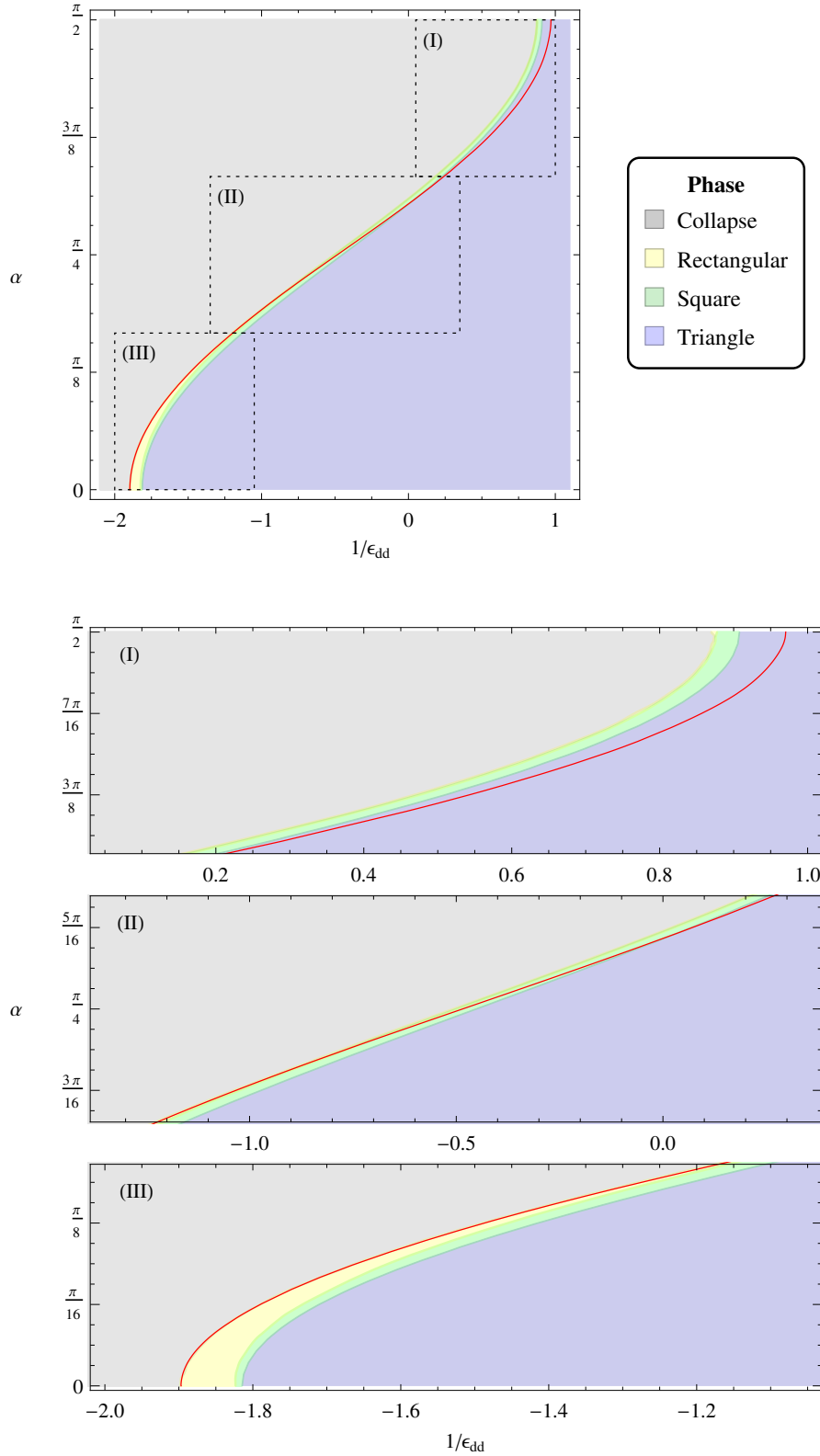


Figure 4.2: *Top:* Plot showing the optimal lattice geometry in dipolar BECs as a function of the polarisation angle α and the relative interaction strength $1/\epsilon_{dd}$. The length scales l_ρ , l_z and σ are assumed to satisfy the relations in row (a) of Table 3.1. The region to the left of the red line is where $E_{\text{int}} < 0$. *Bottom:* Magnified view of the plot above in regions (I), (II) and (III).

Chapter 5

Conclusions, ongoing and future work

5.1 Conclusions

In this thesis, I have outlined a method for analysing vortex lattice geometry in quasi-2D BECs in the fast-rotating limit. The basic idea behind the method was to construct a variational ansatz for the vortex lattice ground state, evaluate the corresponding energy in the rotating frame, and minimise with respect to the variational parameters. In doing so, it was possible to determine the energetically favourable vortex lattice geometry based on the optimal values of the variational parameters.

In conducting the vortex lattice analysis, a number of assumptions were made about the properties of the BEC and the vortex lattice itself. Specifically, I assumed that the BEC was in the limit of fast rotation, weak interactions and strong longitudinal trapping, and that the vortex lattice was uniform and centred on the axis of rotation. With these assumptions, I was able to derive a relatively simple ansatz for the vortex lattice ground state. This enabled me to proceed reasonably far with the problem analytically, however when it came to the final step of energy minimisation I resorted to a numerical treatment.

Using this method, I analysed vortex lattice geometry in both non-dipolar and dipolar BECs. I began by confirming the well-established result that vortex lattices in non-dipolar BECs are triangular. I then considered dipolar BECs, for which I discovered three possible vortex lattice geometries: triangular, square or rectangular. In general, the triangular lattice geometry is favoured in dipolar BECs with dominant positive local interactions ($1/\epsilon_{\text{dd}} \gtrsim 1$), whereas the square and rectangular lattices are favoured in those with dominant non-local interactions ($|1/\epsilon_{\text{dd}}| \lesssim 1$). In addition to these three vortex lattice geometries, I also found that it is sometimes favourable for the vortex lattice to collapse. This appears to occur in dipolar BECs with large negative local interactions ($1/\epsilon_{\text{dd}} \lesssim -1$), although the analysis is not necessarily reliable in this regime.

The results that I have obtained appear to qualitatively agree with previous analytical studies of vortex lattice geometry in dipolar BECs with on-axis polarisation by Zhang and Zhai [1] and Cooper et al. [2]. In this work, however, I have additionally considered the

case of arbitrary dipole polarisation. I find that the direction of the dipole polarisation has a significant effect on the favoured vortex lattice geometry. In particular, the rectangular lattice ceases to exist as the dipole polarisation is tilted off-axis. I also observe a shift in the vortex lattice phase boundaries in the positive $1/\epsilon_{\text{dd}}$ direction as the dipole polarisation is tilted further and further off-axis.

This is the first time that anyone has considered vortex lattice geometry for the case of arbitrary dipole polarisation. By extending my analysis to treat this case, I have been able to investigate vortex lattice geometry over a larger range of the parameter space of dipolar BECs than has been previously considered. My results should be useful in guiding future experiments and simulations regarding vortex lattice geometry in dipolar BECs.

5.2 Ongoing work

Throughout this thesis, I have assumed that the ansatz for the vortex lattice ground state derived in Chapter 2 provides an appropriate description of vortex lattices in both non-dipolar and dipolar BECs. There appears to be no reason to doubt the validity of this ansatz, so long as the following conditions are met:

- (i) the BEC is in the LLL,
- (ii) the BEC is cylindrically symmetric, and
- (iii) the vortex lattice is uniform and centred on the axis of rotation.

Conditions (i) and (iii) appear to be reasonable for both non-dipolar and dipolar BECs within the scope of our initial assumptions (fast rotation, weak interactions and strong longitudinal trapping). Condition (ii), however, is somewhat problematic. Although non-dipolar BECs and dipolar BECs with on-axis polarisation do have cylindrical symmetry, dipolar BECs with off-axis polarisation do not. To see this, one may note that the Hamiltonian for a dipolar BEC with off-axis polarisation depends on the azimuthal angle. One may also understand the broken cylindrical symmetry from a more physical perspective by picturing the elongation of a dipolar BEC along the polarisation direction — an effect that is well-known from experiment [38]. Clearly, if the elongation occurs along any direction other than the z -direction, as it does for the case of off-axis polarisation, the cylindrical symmetry about the z -axis will be broken.

It is unknown whether the broken cylindrical symmetry for the case of off-axis polarisation has any effect on the preferred vortex lattice geometry. In theory, I should be able to test this by redoing the vortex lattice analysis using an ansatz that does not assume cylindrical symmetry. In practice, however, we shall see that this adds considerable complexity to the problem which is difficult to overcome.

5.2.1 A new ansatz for the vortex lattice ground state

Although it is no longer appropriate to assume cylindrical symmetry for the case of off-axis polarisation, there is still another useful symmetry that we may exploit: reflection symmetry. For our choice of coordinate system, this reflection symmetry occurs about the xz -plane — the plane which contains both the polarisation vector $\hat{\mathbf{p}}$ and the axis of rotation. It is possible to prove this mathematically by noting that the Hamiltonian $H_0 + V$ (in particular the $U_{\text{dd}}(\mathbf{r})$ term) is invariant under the replacement $\phi \rightarrow -\phi$.

In order to derive a new ansatz for the vortex lattice ground state which assumes reflection symmetry, we only need to make some minor modifications to the derivation for the cylindrically symmetric case which was given in Section 2.2.3. Specifically, we find that it is necessary to introduce two new variational parameters: λ and ϑ .

The parameter λ is required to describe the deviation of the condensate cloud from cylindrical symmetry. It is defined as the ratio of the width of the condensate cloud along the y -direction divided by the width along the x -direction. If the density profile of the cloud is expressed in the form $\exp(-x^2/\sigma_x^2 - y^2/\sigma_y^2)$, then the aspect ratio would be written as $\lambda = \sigma_y/\sigma_x$. For a cylindrically symmetric BEC, the width of the cloud along the x - and y -directions must be the same, which implies that $\lambda = 1$. However, for a non-cylindrically symmetric condensate, it must be the case that $0 < \lambda < 1$ or $\lambda > 1$. In the current context, it is expected that the optimal value of λ will satisfy $0 < \lambda < 1$. This is because we know that the dipolar BECs elongate along the direction of polarisation, which implies that $\sigma_x > \sigma_y$.

The other new parameter, ϑ , is required to allow the vortex lattice to adopt any orientation with respect to the polarisation direction $\hat{\mathbf{p}}$. It is defined to be the angle between the first lattice basis vector, \mathbf{b}_1 , and the projection of the dipole polarisation onto the plane of rotation, $\hat{\mathbf{p}}_{\perp}$. For a cylindrically symmetric BEC, we do not expect the energy to vary as a function of the orientation of the vortex lattice, so ϑ may be arbitrarily set to zero. However, for a non-cylindrically symmetric BEC, it is conceivable that the energy may depend on ϑ . Here, we may additionally use reflection symmetry about the x -axis to limit the possible values of ϑ to 0 or $\frac{\pi}{2}$.

By modifying the derivation of the ansatz for the vortex lattice ground state to incorporate the new λ and ϑ parameters, it is possible to show that the condensate density must be of the following form:

$$n(\boldsymbol{\rho}) = \frac{2N\lambda}{\pi\sigma^2(1+\lambda^2)} e^{-\frac{2}{1+\lambda^2}\left(\frac{\lambda^2x^2+y^2}{\sigma^2}\right)} \sum_{\mathbf{q}} \bar{g}_{\mathbf{q}} e^{i\mathbf{q}\cdot\hat{R}_{\vartheta}\boldsymbol{\rho}}, \quad (5.1)$$

where \hat{R} represents the standard two-dimensional rotation operator and $\bar{g}_{\mathbf{q}}$ is redefined so that

$$\bar{g}_{\mathbf{q}} = g_{\mathbf{q}} / \sum_{\mathbf{v}} g_{\mathbf{v}} e^{-\frac{\sigma^2(1+\lambda^2)}{8}[(\mathbf{v}\cdot\hat{R}_{\vartheta}\hat{\mathbf{x}})^2/\lambda^2 + (\mathbf{v}\cdot\hat{R}_{\vartheta}\hat{\mathbf{y}})^2]}.$$

5.2.2 Re-evaluating the condensate energy

Now that we have a new ansatz for the two-dimensional condensate density, $n(\boldsymbol{\rho})$, we must re-evaluate the entire quasi-2D energy functional: $E[n] = E_0[n] + E_{\text{cont}}[n] + E_{\text{dd}}[n]$. Omitting the details of the calculation, we find that the single-particle energy contribution $E_0[n]$ evaluates to:

$$E_0(\lambda) = N(\hbar\Omega + \frac{1}{2}\hbar\omega_z) + \frac{N\hbar\sigma^2(\omega_\rho^2 - \Omega^2)}{2\Omega l_\rho^2} \left(\frac{1 + \lambda^2}{2\lambda}\right)^2, \quad (5.2)$$

and the interaction energy contribution, $E_{\text{int}}[n] = E_{\text{cont}}[n] + E_{\text{dd}}[n]$, evaluates to:

$$E_{\text{int}}(\tau, \eta, \lambda, \vartheta) = \frac{N^2 C_{\text{dd}}}{3(2\pi)^{\frac{3}{2}} l_z^3} \left[\left(\frac{1 + 3\cos(2\alpha)}{2} + \frac{1}{\epsilon_{\text{dd}}} \right) \left(\frac{l_z}{\sigma} \right)^2 \mathcal{I}(\tau, \eta, \lambda) + \mathcal{W}(\tau, \eta, \lambda, \vartheta) \right]. \quad (5.3)$$

Here \mathcal{I} and \mathcal{W} are slightly modified compared to definitions given in previous chapters. After making appropriate approximations, we find that

$$\mathcal{I}(\tau, \eta, \lambda) \approx \frac{\lambda}{1 + \lambda^2} \sum_{\mathbf{q}} (\bar{g}_{\mathbf{q}})^2 \quad (5.4)$$

and

$$\mathcal{W}(\tau, \eta, \lambda, \vartheta) \approx \sum_{\mathbf{q}} (\bar{g}_{\mathbf{q}})^2 \exp \left[-\frac{\sigma^2(1 + \lambda^2)}{2} \left(\frac{(q_x^{-\vartheta})^2}{\lambda^2} + (q_y^{-\vartheta})^2 \right) \right] A_2 \left(\frac{2q_x^{-\vartheta}}{\lambda}, 2q_y^{-\vartheta} \right), \quad (5.5)$$

where

$$A_2(q_x, q_y) = \frac{3}{2\sqrt{\pi}} \int_0^\infty du \int_0^{2\pi} du_\phi \left\{ u^2 e^{u^2} \text{erfc}(u) (\sin^2 \alpha \cos^2 u_\phi - \cos^2 \alpha) \right. \\ \left. \times \exp \left[-\frac{\sigma^2(1 + \lambda^2)}{2l_z^2} \left(\frac{u^2 \cos^2 u_\phi}{\lambda^2} + u^2 \sin^2 u_\phi + \frac{l_z q_x u \cos u_\phi}{\sqrt{2}\lambda} + \frac{l_z q_y u \sin u_\phi}{\sqrt{2}} \right) \right] \right\}. \quad (5.6)$$

Hence we have given an expression for the total energy, $E(\tau, \eta, \lambda, \vartheta) = E_0(\lambda) + E_{\text{int}}(\tau, \eta, \lambda, \vartheta)$, of a non-cylindrically symmetric dipolar BEC in the vortex lattice ground state. We have emphasised, through our choice of notation, that this expression depends on four variational parameters: τ , η , λ and ϑ . As a result, it is now necessary to perform the energy minimisation with respect to λ and ϑ , in addition to τ and η . This makes the numerical minimisation significantly more challenging, because the global minimum now exists in a much larger variational parameter space.

In addition to the increased size of the variational parameter space, we must also contend with convergence issues in numerically evaluating $\mathcal{W}(\tau, \eta, \lambda, \vartheta)$ as we did in previous chapters. Once again, these issues stem from the poor convergence properties of the integral that defines $A_2(q_x, q_y)$ in Equation (5.6). Previously, we dealt with this problem by analytically evaluating the integral over u_ϕ and breaking up the remaining integral over u into an infinite series of simpler, tractable integrals. Unfortunately, this approach is no longer effective due to the broken cylindrical symmetry of the integrand. After exploring a number

of alternative approaches, the best option we could find was to do the integral over u analytically (surprisingly it is possible) and the integral over ϕ_u numerically. Convergence is still slow with this approach, because the integral over ϕ_u is highly oscillatory, however it is a vast improvement on evaluating the entire double integral over u and ϕ_u numerically.

5.2.3 Optimal vortex lattice geometry

In theory, we can use the non-cylindrically symmetric expression for the condensate energy, given above, to re-calculate the optimal vortex lattice geometry in dipolar BECs with off-axis polarisation. Unfortunately, however, this is not feasible from a computational perspective, because our implementation of the condensate energy takes too long to converge to sufficient accuracy. Even if we include a relatively small number of terms in the Fourier decomposition, say $M = 3$, our implementation takes of order minutes to evaluate for a given combination of variational parameters. If we increase the number of terms to $M = 15$, which is required to explore the parameter space where τ and η approach zero, then the evaluation time exceeds one hour. This means that it is impractical to minimise $E(\tau, \eta, \lambda, \vartheta)$ with respect to τ , η , λ and ϑ , because doing so requires hundreds of evaluations of E , each of which already takes an exceedingly long time.

Although there are severe computational limitations surrounding the minimisation of our new expression for the condensate energy, we may still make some meaningful calculations if we restrict our attention to triangular and square lattices only. By restricting our attention in this way, we may avoid τ and η approaching zero, which permits us to set $M = 3$, thereby reducing the computation time to a manageable level. One calculation that we may do within these restrictions, is to minimise the energy with respect to λ and ϑ for both triangular and square lattices. In doing so, we can expect to gain some insight on whether the optimal values of λ and ϑ vary between the two different lattice geometries.

Since the computation is still quite slow (even with $M = 3$), we shall only perform the energy minimisation at two points in the $(1/\epsilon_{\text{dd}}, \alpha)$ parameter space: $(0.9, \frac{\pi}{2})$ and $(0.95, \frac{\pi}{2})$. We have chosen these points for two reasons:

- (i) They occur at $\alpha = \frac{\pi}{2}$, where the deviation from cylindrical symmetry is expected to be most prominent.
- (ii) They are well within the square and triangular lattice regions based on the results of Figure 4.1. This means that it is less likely that a rectangular lattice would become favourable at these points, even after accounting for the deviation from cylindrical symmetry.

In performing the energy minimisation with respect to λ and ϑ at these two points, we should technically consider the total energy $E(\tau, \eta, \lambda, \vartheta) = E_0(\lambda) + E_{\text{int}}(\tau, \eta, \lambda, \vartheta)$ since both the single-particle and interaction energy contributions depend on λ . For now, however, we shall only look at the role of the interaction energy contribution, since it is the only part of the energy that depends on the dipole polarisation. The results of the minimisation are given in Table 5.1.

<i>Cylindrically symmetric ansatz</i>			<i>New ansatz</i>		
$1/\epsilon_{\text{dd}}$	Phase	E_{int}	Phase	Optimal λ	E_{int}
0.90	Square	-4784.22	Square	0.93	-4979.49
0.90	Triangular	-4775.18	Triangular	0.93	-4788.31
0.95	Square	-1331.22	Square	0.78	-1377.22
0.95	Triangular	-1382.86	Triangular	0.78	-1426.81

Table 5.1: Results of the minimisation of the new expression for E_{int} with respect to λ and ϑ for triangular and square lattices at two values of $1/\epsilon_{\text{dd}}$ with $\alpha = \frac{\pi}{2}$. The optimal value of ϑ is not included in the table, because E_{int} was found to be independent of ϑ . The results show that the optimal value of λ is the same for both triangular and square lattice geometries.

Looking at the results, we may conclude that the variational parameter ϑ is essentially irrelevant, since the minimum value of $E_{\text{int}}(\tau, \eta, \lambda, \vartheta)$ is found to be the same for any choice of ϑ . This suggests that the orientation of the vortex lattice is unaffected by the broken cylindrical symmetry due to the off-axis polarisation. In contrast, we find that the optimal value of λ does deviate from the cylindrically symmetric value of 1. At both points we have considered the optimal value is found to be less than 1, which indicates that the BEC has stretched along the direction of polarisation. Interestingly, however, we find that the optimal value of λ does not depend on whether the lattice geometry is square or triangular — it is the same for the square and triangular lattice at each of the points we considered. This provides decent evidence that λ is independent of the vortex lattice geometry (although we have not yet been able to prove this for *all* possible vortex lattice geometries). Consequently, we may tentatively claim that the vortex lattice geometry is unlikely to be affected by the broken cylindrical symmetry due to the off-axis polarisation¹. As such, we can be reasonably confident that our previous results regarding vortex lattice geometry for the case of off-axis polarisation are correct, even though we did not take the broken cylindrical symmetry into account.

5.3 Future work

The work that I have begun regarding broken cylindrical symmetry for the case of off-axis polarisation warrants further investigation. Possible future directions could include making a perturbative expansion in λ , looking for a more efficient implementation of $E_{\text{int}}(\tau, \eta, \lambda, \vartheta)$, or pushing through with calculations on a more powerful computer. In addition, it would also be worthwhile to conduct numerical simulations of the GP equation to check the results I have obtained using an alternative method.

¹Since λ quantifies the extent to which the cylindrical symmetry is broken

Bibliography

- [1] J. Zhang and H. Zhai, Physical Review Letters **95**, 200403 (2005).
- [2] N. R. Cooper, E. H. Rezayi, and S. H. Simon, Physical Review Letters **95**, 200402 (2005).
- [3] A. Einstein, Sitzber. Kgl. Preuss. Akad. Wiss. **3** (1925).
- [4] M. H. Anderson, J. R. Ensher, M. R. Matthews, C. E. Wieman, and E. A. Cornell, Science **269**, 198 (1995).
- [5] K. B. Davis, M. Mewes, M. R. Andrews, N. J. van Druten, D. S. Durfee, D. M. Kurn, and W. Ketterle, Physical Review Letters **75**, 3969 (1995).
- [6] Nobel Media AB, *The Nobel Prize in Physics 2001*, Nobelprize.org, (2013) http://www.nobelprize.org/nobel_prizes/physics/laureates/2001/ (visited on 05/07/2014).
- [7] A. Griesmaier, J. Werner, S. Hensler, J. Stuhler, and T. Pfau, Physical Review Letters **94**, 160401 (2005).
- [8] M. Lu, N. Q. Burdick, S. H. Youn, and B. L. Lev, Physical Review Letters **107**, 190401 (2011).
- [9] E. P. Gross, Il Nuovo Cimento Series 10 **20**, 454 (1961).
- [10] L. P. Pitaevskii, Soviet Physics JETP **13**, 451 (1961).
- [11] A. L. Fetter and J. D. Walecka, *Quantum Theory of Many-Particle Systems* (Courier Dover Publications, Mar. 8, 2012), 646 pp.
- [12] C. Chin, R. Grimm, P. Julienne, and E. Tiesinga, Reviews of Modern Physics **82**, 1225 (2010).
- [13] S. Yi and L. You, Physical Review A **61**, 041604 (2000).
- [14] S. Yi and L. You, Physical Review A **63**, 053607 (2001).
- [15] L. P. Pitaevskii and S. Stringari, *Bose-Einstein Condensation* (Oxford University Press, Apr. 3, 2003), 392 pp.
- [16] A. L. Fetter and A. A. Svidzinsky, Journal of Physics: Condensed Matter **13**, R135 (2001).
- [17] D. H. J. O'Dell and C. Eberlein, Physical Review A **75**, 013604 (2007).
- [18] R. P. Feynman, in *Progress in Low Temperature Physics*, Vol. V, 1st ed. (North-Holland, Ch. 11, 1955).

-
- [19] A. Abrikosov, *Journal of Physics and Chemistry of Solids* **2**, 199 (1957).
- [20] D. Cribier, B. Jacrot, L. M. Rao, and B. Farnoux, *Physics Letters* **9** (1964).
- [21] T.-L. Ho, *Physical Review Letters* **87**, 060403 (2001).
- [22] I. Coddington, P. C. Haljan, P. Engels, V. Schweikhard, S. Tung, and E. A. Cornell, *Physical Review A* **70**, 063607 (2004).
- [23] G. Watanabe, G. Baym, and C. J. Pethick, *Physical Review Letters* **93**, 190401 (2004).
- [24] A. Aftalion, X. Blanc, and J. Dalibard, *Physical Review A* **71**, 023611 (2005).
- [25] I. Coddington, P. Engels, V. Schweikhard, and E. A. Cornell, *Physical Review Letters* **91**, 100402 (2003).
- [26] G. Baym, *Physical Review Letters* **91**, 110402 (2003).
- [27] P. Engels, I. Coddington, P. C. Haljan, V. Schweikhard, and E. A. Cornell, *Physical Review Letters* **90**, 170405 (2003).
- [28] S. Yi and H. Pu, *Physical Review A* **73**, 061602 (2006).
- [29] D. A. Butts and D. S. Rokhsar, *Nature* **397**, 327 (1999).
- [30] J. R. Abo-Shaeer, C. Raman, J. M. Vogels, and W. Ketterle, *Science* **292**, 476 (2001).
- [31] E. J. Mueller and T.-L. Ho, *Physical Review Letters* **88**, 180403 (2002).
- [32] L. D. Landau and E. M. Lifshitz, *Mechanics*, *Teoreticheskaya fizika 1* (Pergamon Press, 1960), 165 pp.
- [33] V. Schweikhard, I. Coddington, P. Engels, V. P. Mogendorff, and E. A. Cornell, *Physical Review Letters* **92**, 040404 (2004).
- [34] V. M. Pérez-García, H. Michinel, and H. Herrero, *Physical Review A* **57**, 3837 (1998).
- [35] N. K. Wilkin, J. M. F. Gunn, and R. A. Smith, *Physical Review Letters* **80**, 2265 (1998).
- [36] J. M. Gerton, D. Strekalov, I. Prodan, and R. G. Hulet, *Nature* **408**, 692 (2000).
- [37] U. R. Fischer, *Physical Review A* **73**, 031602 (2006).
- [38] T. Lahaye, J. Metz, B. Fröhlich, T. Koch, M. Meister, A. Griesmaier, T. Pfau, H. Saito, Y. Kawaguchi, and M. Ueda, *Physical Review Letters* **101**, 080401 (2008).